AD-A167 918 ACTA AERONAUTICA ET ASTRONAUTICA SINICA (SELECTED ARTICLES)(U) FOREIGN TECHNOLOGY DIV WRIGHT-PATTERSON AFB OH H ZHANG ET AL. 09 MAY 86 FTD-ID(RS)T-0109-86 1/1

UNCLASSIFIED F/G 20/4 NL

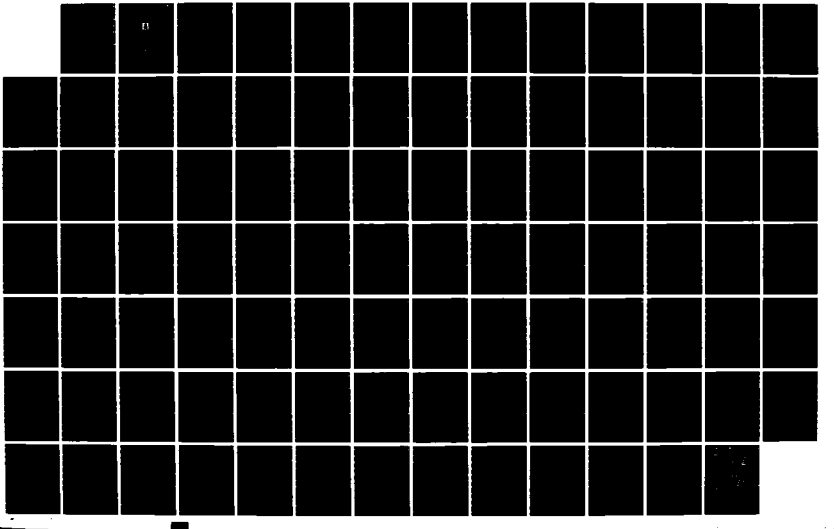

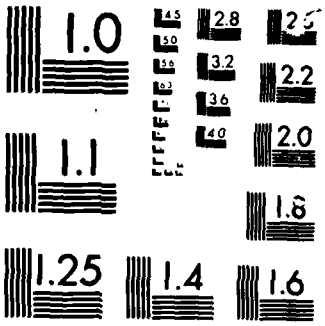

MICROCOPY CHART

FTD-ID(RS)T-0109-86

AD-A167 918

FOREIGN TECHNOLOGY DIVISION

ACTA AERONAUTICA ET ASTRONAUTICA SINICA

(Selected Articles)

DTIC FILE COPY

Approved for public release;
Distribution unlimited.

HUMAN TRANSLATION

FTD-ID(RS)T-0109-86 9 May 1986

MICROFICHE NR: FTD-86-C-001813

ACTA AERONAUTICA ET ASTRONAUTICA SINICA (Selected Articles)

English pages: 90

Source: Hang Kong Xuebao, Vol. 6, Nr. 4, 1985, pp. 301-312; 321-334; 362-370; 379-384; 393-404

Country of origin: China
Translated by: SCITRAN
F33657-84-D-0165
Requester: FTD/TQTA

PREPARED BY:

TRANSLATION DIVISION
FOREIGN TECHNOLOGY DIVISION
WPAFB, OHIO.

Table of Contents

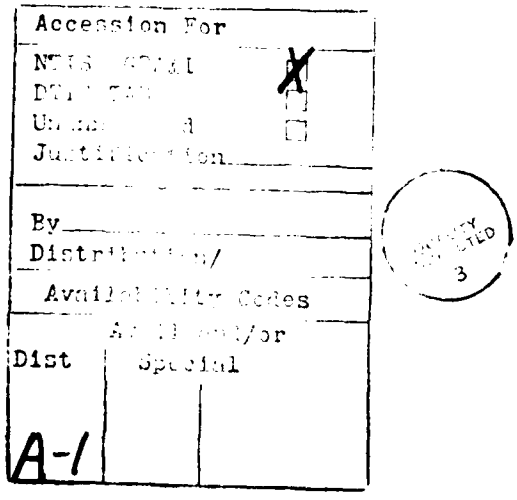

GRAPHICS DISCLAIMER

All figures, graphics, tables, equations, etc. merged into this translation were extracted from the best quality copy available.

ADVANCES IN THE STUDY OF SEPARATED FLOWS

by

ZHANG Hanxin
(Chinese aerodynamic Research and Development Center)

ABSTRACT

This paper briefly reviews the separation criteria for two-dimensional unsteady flows and three-dimensional steady viscous flows, and discusses the flow patterns near the separation point or the separation line. An introduction of the author's work is given.

1. INTRODUCTION

During the past decade or so, much attention has been paid to the studies on separation flows with a need in the development of motor vehicles. Two interesting subjects among these studies are the origin of separation and the characteristic features of the two-dimensional unsteady and three-dimensional steady flows. Moore(1957)(1), Rott(1956)(2) and Sears(1956)(3) pointed out in late 1950's that the Prandtl's separation criterion for two-dimensional unsteady flow was no longer valid for two-dimensional

Received September 20, 1984.

unsteady flow. Instead, they independently proposed later the so-called MRS separation criterion (the velocity cross section near the corresponding separation point is called the MRS cross section). Then, Sears and Telionis(1971)(4) pointed out that solution to the unsteady boundary-layer equation exhibited a Goldstein-type singularity at separation. From that, the "singular point separation criterion" was proposed. Vidal(1959)(5) and Ludwig(1964)(6) verified the MRS criterion in a steady flow experiment on a moving wall. The MRS criterion and the singular point separation criterion were also verified under the downstream-moving wall conditions (or the wall did not move, but the separation point moved upstream) by Telionis and Werle(1973)(7) in numerical solutions to the steady boundary-layer on a downstream-moving wall; by Telionis, Tsahalis and Werle(1973)(8) with the difference solution to the unsteady Howarth's linear deceleration boundary-layer; and by Williams and Johnson(1974)(9), Williams(1981)(10), and C. T. Wang and S. F. Shen (1978)(11) in the semisimilar solution to the Howarth's linear deceleration-type and Falkner-Skan-type unsteady boundary-layers. In the case of upstream-moving walls, however, the MRS criterion was not verified by Danberg and Fansler(12) with the similar solution to the steady boundary layers; by Tsahalis(13) in the numerical solution to the unsteady boundary layers; and by Inoue(14) with the numerical solution to the simplified NS equation. Recently, Dommelen and Shen calculated the instantaneously-starting boundary-layer flows on a cylindrical surface using Lagrange's method. They found that when the cylinder moved from the starting point through a distance, 0.75 of its diameter, a singular point appeared at 110^{o} from the

front stagnation point, then moved forward along the surface at a speed 0.52 times that of the cylinder, and finally stopped at 104.5° steady position. They also found that although the criterion could serve at the singular point, the friction stress curves were smooth and even, while the displacement thickness increased dramatically. Therefore, the singular point was not of the Goldstein-type, which was controlled by the viscous friction force (also called a viscous singular point), but of another type, which was called inviscid singular point. K. C. Wang's unsteady similar calculation has confirmed Dommelen and Shen's results to some extent. However, according to Cebeci(18), Dwyer and Sherman (19), within a limited period of time, there is no singular point in an instantaneously-starting cylinder.

In 1950's. research work was conducted on the origin of separation and the boundary line (separation line) patterns in the separation region for three-dimensional steady flows. To date, a lot of theories, experimental work(20-27), and review papers(28-30) are available on the topic. However, Brown and Stewartson(28), and Williams(30), et al. pointed out that there still existed a lot of controversy on this subject. For example, about the characteristics of the separation line, Eichelbrenner and Oudart(31); Maskell(20); and K. C. Wang believed ealier that the separation line was an envelope of the limiting streamlines on a wall. However, according to Legendre(21,32), Lighthill(22) (who developed the concept of friction force lines which are usually considered to be equivalent to the limiting streamlines) and Hunt(33); and Tobak and Peake(34-36), a separation line is a limiting streamline on the wall and except

for the singular point, it is impossible for the nearby limiting streamlines to intersect the separation line which is a "convergent asymptote" within a limited distance. Also, Brown and Stewartson(28) questioned the possibility for the separation line of the flow described in the boundary-layer equation to exhibit a Goldstein-type singularity similar to the separation point of the two-dimensional unsteady flow. Recently, Cousteix's work using approximate integral relation techniques shows the possibility of exhibiting such a singularity.

The origin and terminal of the three-dimensional separation line are other interesting topics. Legendre (21) and Lighthill (22) suggested that the origin of the separation line should be a saddle point, while Maskell(20), K. C. Wang(24), et al. found through their experimentation and calculations that there were two types of separation origin: bubble and vortex-layer separation, as defined by Maskell; open- and closed-type separation, as defined by K. C. Wang; and the integral and partial separation, as recently defined by Tobak, Peake, et al. For bubble or closed-type (or integral) separation, the origin of the separation line is actually a saddle singular point, but the origin of vortex or open-type (or partial) separation is not a singular point. Research on the termination of the separation line shows that, except for the singular point of zero friction stress, the separation line changes continuously, and when it meets a focus or a node, the line terminates at such a singular point. Because of the connection of the singular point with separation, Legendre(21), Oswatitsch(23), and Lighthill(22) studied the singular point distribution on a material surface using topological techniques.

Hunt(33), et al. extended the material surface singular point and topological analysis to include body cross-section in the outside flow field, and proposed semi-nodal and semi-saddle point concepts. Tobak and Peake(34) further investigated the applicability of topology to the three-dimensional separation flow and put forward topological structure and structure stability theories(35,36). The authors(38) and Liu Moujie, et al. also anslyzed these singular points.

In summary, the following questions concerning the origin of separation and the patterns of the two-dimensional unsteady and three-dimensional steady flows need to be answered.

(1) For two-dimensional unsteady flow, are MRS criterion and the singular point separation criterion universal and equivalent to each other? Does the singular point given by the singular point separation criterion exhibit viscous or inviscid behavior? Does the separation singular point appear after a limited duration of time?

(2) For three-dimensional steady flow, what are the separation conditions? Is the separation line an envelope of the wall limiting streamlines or an asymptote of the limiting streamlines themselves and nearby ones? Does the separation line for the flow described in the steady boundary-layer equation exhibit a singularity? How does the separation line originate and terminate? What are the singular point distribution and the separation line patterns at the singular point?

Moreover, according to K.C. Wang's analogue separation criterion, under certain conditions, the two-dimensional unsteady flow can

be analogized as the three-dimensional steady flow, and the separation criteria for the two-dimensional unsteady flow and three-dimensional steady flow should be transformed from each other. It is worth investigating if a transformation of the separation criteria now available for the two types of flows can be performed.

The objective of this paper is to discuss and review the above-mentioned problems, and to introduce the author's work on the topic.

2. TWO-DIMENSIONAL UNSTEADY FLOWS

Sears, Moore and Hartunian pointed out the similarities between unsteady flow over fixed walls and steady flow over moving walls. Sears defined separation of two-dimensional unsteady flow as "the appearance of the stagnation point and the separation line which separates the boundary layer and the wake in a coordinate system moving with the separation point"(see literature (3-13)). 303

According to this definition, a separation point is of stagnation type. Moore, Rott and Sears have also provided the flow patterns near the separation point (MRS sketches), as shown in Fig. 1. In the figure, (a) corresponds to steady flow over fixed walls, and (b) and (c) correspond to the moving wall condition. After a careful analysis, O'Brien pointed out in 1981 that unsteady laminar separated flow exhibited three patterns which were similar to those of a steady flow, as shown in Fig. 2. When only the vicinity of the stagnation point is considered, three O'Brien's patterns are completely consistent with the MRS sketches. Most studies on two-dimensional unsteady separated flows today start with this definition of separation and these separation sketches.

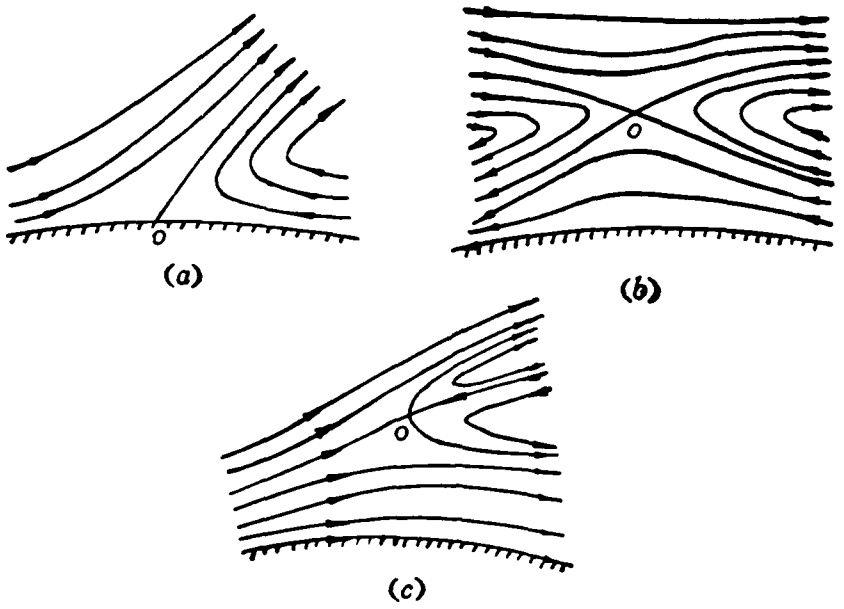

Fig. 1 MRS' sketches

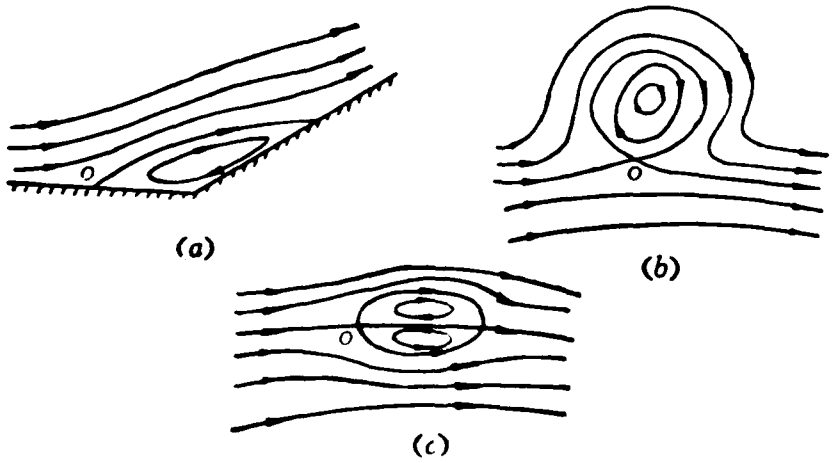

Fig. 2 Separation sketches given by O'Brien

In the two-dimensional unsteady separated flow studies, one of the important topics is criteria for separation. The following are those suggested in the literature.

(1) MRS (Moore, Rott and Sears) criterion(1-3). Conditions for separation to appear are that at the separation point

$$u_0 = 0 \qquad \left(\frac{\partial u}{\partial y}\right)_0 = 0 \tag{2.1}$$

where u is the velocity component in x direction; y, the direction perpendicular to the material surface; and xoy, the coordinate system moving with the separation point.

(2) O'Brien's criterion(42). The separation conditions are that at the separation point

$$u_0 = 0 \qquad \Omega_0 = \left(\frac{\partial v}{\partial x} - \frac{\partial u}{\partial y}\right)_0 = 0 \tag{2.2}$$

where v is the velocity component in y direction.

(3) Singular point separation criterion (Sears and Telionis) (4). The separation conditions for the flow described in the boundary-layer equation are

$$u_0 = 0 \qquad \left(\frac{\partial \tau}{\partial x}\right)_0 \to \infty \tag{2.3}$$

304

where τ is the partial shear stress, namely, the separation point is a Goldstein-type singular point.

(4) Singular-type parameter criterion (Fansler and Danberg) (43). Condition for the boundary-layer separation is that at the separation point

$$\left(\frac{dH}{dK}\right)_0 \to \infty \tag{2.4}$$

where H is the ratio of displacement thickness of the boundary layer to the momentum thickness; and K, the ratio of the energy thickness to the momentum thickness.

(5) Analogue separation criterion (K. C. Wang)(17) states that

for two-dimensional unsteady flow, the separation criterion can be established based on that for three-dimensional flow.

In addition, C. T. Wang and S. F. Shen(11) also proposed a separation criterion which is similar to MRS criterion.

Many investigators have been devoted to examining and evaluating the above separation criteria. It is generally accepted that MRS criterion and zero vortex criterion are valid under conditions with flow over downstream-moving walls, but lead to erroneous results in cases of flow over upstream-moving walls; zero vortex criterion is not valid especially when the streamlines passing through the separation point are not normal to each other(42). The singular point separation criterion and singular-type parameter criterion can only be applied to certain boundary layer flows. The analogue separation criterion is also dependent on the criterion for separation of three-dimensional steady flow, which is still under discussion. In view of the above-mentioned facts, we studied the separation of incompressible viscous flow using singular point theory for differential equations based on Sears' definition of separation, and give the following conditions for separation(40,41):

(1) In a viscous flow field, if $u_0=v_0=0$ at point "o", and

$$F=\left(\frac{\partial u}{\partial x}\right)_0^2+\left(\frac{\partial v}{\partial x}\right)_0\left(\frac{\partial u}{\partial y}\right)_0>0 \qquad (2.5)$$

is satisfied, then point "o" is a separation point. If $F<0$, point "o" is not a separation point. Here, xy is the coordinate system moving with "o", and u and v are velocity components.

(2) If $u_0=v_0=0$ and $F=0$ at point "o", and $\Omega_0=0$ and

$$(q^2+R^3)/q^2=0 \qquad (2.6)$$

are satisfied, where $q=\left(\frac{C_1}{D_1}\right)^3-\frac{3}{2}\frac{B_1}{D_1}\frac{C_1}{D_1}-\frac{1}{2}\frac{A_1}{D_1}$, $R=-\left(\frac{C_1}{D_1}\right)^2+\left(\frac{B_1}{D_1}\right)\neq 0$

and $A_1=(\partial^2 v/\partial x^2)_0$, $B_1=(\partial^2 u/\partial x^2)_0$, $C_1=(\partial^2 u/\partial x\partial y)_0$, $D_1=(\partial^2 u/\partial y^2)_0$, then "o" is a separation point.

Based on this study, we can draw the following conclusions (41):

(1) From condition (1), there exists a zero u line (u=0) passing through the separation point. This is corresponding to the MRS sketch in Fig. 1(b). From condition (2), there are two zero u lines passing through the separation point, which correspond to the MRS sketches in Fig. 1(a) and 1(c).

(2) If the MRS conditions hold at point "o", and $\left(\frac{\partial u}{\partial x}\right)_0 \neq 0$ then condition (1) must be satisfied and point "o" is a separation point. Thus, condition (1) contains MRS criterion. In this case, one of the slopes for streamlines passing through "o" is infinity (here $(\partial^2 u/\partial x\partial y)_0$ is not an infinity). Another slope is $\frac{1}{2}\left(\frac{\partial v}{\partial x}\right)_0 / \left(\frac{\partial u}{\partial x}\right)_0$.

(3) If zero vortex criterion holds at point "o" and $\left(\frac{\partial u}{\partial x}\right)_0 \neq 0$ or $\left(\frac{\partial u}{\partial y}\right)_0 \neq 0$, , then condition (1) must be satisfied and "o" must be a separation point. Thus condition (1) contains zero vortex criterion.

(4) For the separated flow which satisfies condition (1), two streamlines passing through separation point "o" are not normal to each other, except that $\Omega_0=\left(\frac{\partial v}{\partial x}\right)_0-\left(\frac{\partial u}{\partial y}\right)_0=0$, .

(5) For steady flow over a fixed wall, if $\left(\frac{\partial u}{\partial y}\right)_0=0$ 及 $\left(\frac{\partial^2 u}{\partial x\partial y}\right)_0 \neq 0$, is satisfied at point "o" on the wall, then condition (2) is satisfied. Thus, point "o" is either a separation point or an attachment point. This is the Prandtl's criterion for steady flows.

(6) For flow described in the boundary layer equations, if at point "o"

$$u_0 = v_0 = 0 \qquad (\partial u/\partial y)_0 = 0$$

and $(\partial u/\partial x)_0 = (\partial v/\partial x)_0 = 0$, , then "o" is generally a Goldstein-type singular point, and condition (2) is satisfied. Therefore, "o" is a separation point, and the slope of one streamline passing through "o" is infinity. This is singular point separation criterion.

(7) For the separated flow satisfying condition (1), MRS and zero vortex conditions are not necessary. But, it is necessary for the separated flow satisfying condition (2).

The above conclusions tell us the following:

(1) The separation criterion conditions based on Sears' definition divide flows into two categories: one with a zero u line and another with two zero u lines. These are consistent with both MRS and O'Brien sketches.

(2) The MRS, zero vortex, singular point separation and Prandtl's criteria are all included in our separation conditions.

(3) For separated flows with one zero u line, the conditions set for MRS and zero vortex criteria for separation are ample but not necessary. Thus, these flows can not represent all kinds of separated flows. For separated flows with two zero u lines, the conditions set for MRS and zero vortex criteria are necessary but not ample. The points where these conditions are satisfied are not necessarily separation points. In a word, MRS and zero vortex criteria are not universal. When calculating steady flow over a downstream-moving wall, many workers found that the MRS conditions held in most cases. This is because flow with two zero u lines appears in most cases where MRS conditions are necessary. It is also found that when steady flow over an upstream-moving wall was cal-

culated, the MRS conditions did not hold in most cases where flows with a zero u line most likely appeared and the MRS conditions were not necessary.

(4) In the case of separated flow described in the boundary-layer equation, if flow shows two zero u lines and the MRS conditions 306
hold, the separation point is generally a Goldstein-type singular point (viscous singular point). In this case, MRS and singular point separation criteria are basically equivalent. However, if flow shows one zero u line, and the MRS conditions hold, inviscid singular point appears with the slope of a streamline passing through the separation point being infinity. Therefore, the singular point separation criterion is not universal. When the MRS conditions hold, either viscous or inviscid singular point may appear.

(5) O'Brien's thinking is correct. He believes that when the streamlines passing through the separation point are not normal to each other, zero-vortex conditions are not satisfied.

3. THREE-DIMENSIONAL STEADY FLOWS

Before three-dimensional steady separated flows over fixed walls are investigated, separation line needs to be defined. In literature, such sketches as shown in Fig. 3 are often used to illustrate the separation line geometrically. The separation line is the intersection of the separated-flow surface and the material surface, and fluid at both sides of the surface flows upward along the surface. With separation line defined in this way, it is not correct to use zero friction stress as a criterion. Recently, two prevalent separation criteria, envelope and asymptote limiting streamline criteria are still under discussion. The necessary con-

ditions proposed by Bai-Zelikovin (44) for three-dimensional steady boundary-layer separation, $\vec{\tau}_w \cdot \mathrm{grad}p = 0$, $\vec{u}_e \cdot \mathrm{grad}p > 0$, where $\vec{\tau}_w$ is the wall friction stress vector; p, the pressure; and $\vec{u}_e$, the velocity of the outside boundary layer, have not yet verified experimentally. It is not correct either that the line where the absolute value of the friction stress is minimum is considered as the separation line. It is, therefore, essential to further investigate conditions for determining the three-dimensional steady flow separation and the flow patterns near the separation line. We have studied this subject and established the following conditions for determining flow separation and the separated flow attachment using above definition of the separation line:

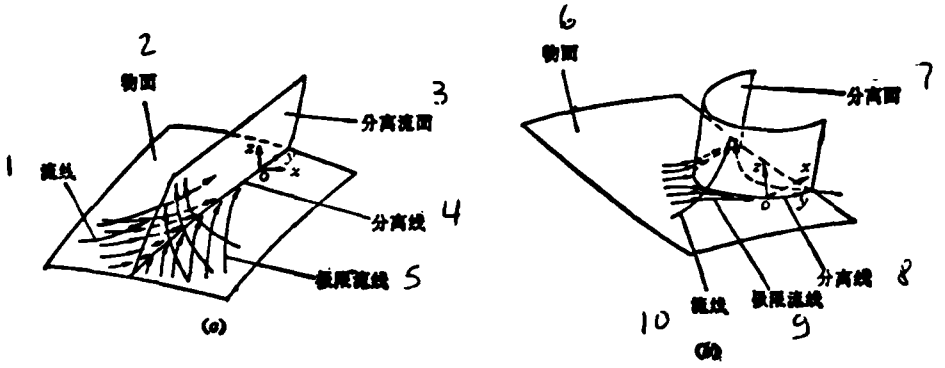

Fig. 3 Illustrating the separation line

1- streamline; 2-material surface; 3- separated flow surface; 4-separation line; 5-limiting streamline; 6-material surface; 7-separated flow surface; 8-separation line; 9-limiting streamline; 10-streamline.

(1) Assuming that xyz is the coordinate system for the normal curves, where y axis is the separation line; and z axis, the normal of the material surface, when flow separation appears, the following conditions at any point "o" on the separation line are satisfied:

$$(\partial u/\partial z)_o = 0 \qquad (\partial^2 u/\partial x \partial z)_o < 0 \tag{3.1}$$

where u is the velocity component in x direction (the normal of the separation line). Obviously, equation (3.1) is an extension of two-dimensional Prandtl's criterion.

(2) When the separated flow attaches the material surface, the following conditions hold at any point "o" on the attachment line:

$$0 < (zexe/u,e) \qquad 0 = ^{\circ}(ze/ue) \tag{3.2}$$

It should be noted that conditions (3.1) and (3.2) hold for NS equation and for the flow described in the boundary-layer equation.

By using the above conditions, we can draw the following con- 307
clusions:

(1) For the flows described in NS equation, the separation line is a limiting streamline; The limiting streamlines around the separation line converge upon it and take it as their asymptote (Fig. 4(a)).

(2) For the flow described in the boundary-layer equation, flow generally exhibits a Goldstein-type singularity in the normal direction of the separation line, and the separation line is the envelope of the limiting streamlines (Fig. 4(c)).

(3) For the flow described in NS equation, the attachment line is a limiting streamline, the limiting streamlines in its vicinity taking the attachment line as their asymptote and generally

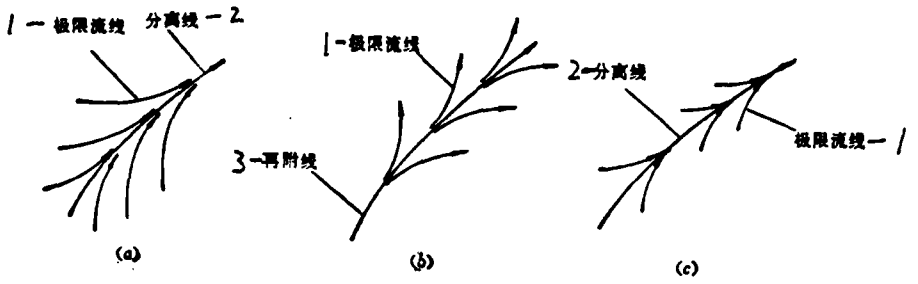

Fig. 4 Limiting streamline patterns near separation and attachment lines (a) Separation line for NS equation; (b) Attachment line for NS equation; (c) Separation line for boundary layer equation.

1-limiting streamline; 2-separation line; 3-attachment line.

diverging outward (Fig. 4(b)).

For Newtonian fluid, since the limiting streamlines are friction stress lines, the above drawn conclusions are also adapted to the friction stress lines.

Based on the above conclusions and by solving the boundary layer equation, C. K. Wang, et al. inevitably arrived at the conclusion that the separation line is an envelope of the limiting streamlines. By solving NS equation as the starting point, however, it can be concluded that the separation line is a convergent asymptote of the limiting streamlines in the vicinity of the separation line. In this sense, therefore, Legendre and Lighthill's ideas are also correct. The reason for this is that the boundary layer approximation results in a singularity of the solution at the separation line, so that aberration of the limiting streamlines occurs and the separation line which should originally be a convergent asymptote of the limiting streamlines under a real condition changes

to an envelope of the limiting streamlines.

In addition, we have discussed the origin and development of the separation line and attachment line, and pointed out that the origin of the separation line assumes two initial states, as shown by Maskell and K. C. Wang: (1) Being originated at a normal point with a nonzero friction stress component. In this case, the separation line behind the origin is a monotonic smooth curve (Fig. 5 (b)). The streamlines ahead can pass through both sides of the curve. (2) Being originated at a singular point, where the friction stress component is zero. In this case, the separation line behind the origin encircles a separation region (Fig. 5(a)) and separates the streamlines ahead from the region. During the backward development of the separation line, this line extends backward until a singular point appears, and terminates at the singular point in a certain state. Based on the singular point theory for a differential equation, it can be verified through analyzing the pattern of the limiting streamlines in the vicinity of the singular point on the separation line that if the origin of the separation line is a singular point, the line can only be of saddle-type, and if the terminal of the separation line is a singular point, the line should be of node- or focus-type.

For the attachment line, the corresponding conclusions can also be drawn: if the origin is a singular point, the line should be of node- or focus-type; and if the terminal is a singular point, the line should be of saddle-type. It can be verified that focus on the separation line or attachment line is a pressure extreme point. Obviously, the singular point is closely related to the

separation line pattern. It is, therefore, significant for the separation line studies to investigate the distribution of singular points on a body surface. At the beginning of 1960's, Davey(46) and Lighthill[22] pointed out that the singular point distribution of the limiting streamline equation obeys the following topological rule: on the surface of a monoconnection body, the total number of the nodes and focal points is 2 more than that of saddles. Later, the topological rule extended from flow over a wall to that beyond the wall. Smith(47), Hunt(33), Tobak, Peake(36), et al. have pointed out that when a monoconnection body is immersed in a flow which is homogeneous at infinite distance:

(1) Assuming that a monoconnection body is constructed by three-dimensional body, B and a flat wall, P, and that P is either an infinite or ring-like surface, then on surfaces B and P, the number of singular points on the limiting streamlines satisfies

$$[(\Sigma N)-(\Sigma S)]_{B+P}=0 \qquad 1-\text{结点,焦点总数}-\text{鞍点总数}-2 \tag{3.3}$$

where 1-total number of the nodes and focal points; and 2-total number of saddles.

(2) On the two-dimensional cross-section cutting a three-dimensional body, the number of the singular points on the streamlines satisfies

$$\left(\Sigma N+\frac{1}{2}\Sigma N'\right)-\left(\Sigma S+\frac{1}{2}\Sigma S'\right)=-1$$

$$1-\text{物面轮廓线外结点,焦点总数}\quad 2-\text{物面轮廓线上的结点、焦点总数(亦称半结点、半焦点总数)}\quad 3-\text{物面轮廓线外鞍点总数}\quad \text{物面轮廓线上鞍点总数(亦称半鞍点总数)}-4 \tag{3.4}$$

where 1-total number of nodes and focal points beyond the outline of the material surface; 2-total number of nodes and focal points on the outline of the material surface (also called the total number of seminodes and semifocuses); 3-total number of saddles beyond the

outline of the material surface; and 4-total number of the saddles on the outline of the material surface (also called total number of semisaddles).

(3) If flow around a three-dimensional is of cone-type, then on the spherical face whose center is the cone-type flows, the number of singular points on the streamlines satisfies

$$\left(\Sigma N+\frac{1}{2}\Sigma N'\right)-\left(\Sigma S+\frac{1}{2}\Sigma S'\right)=0 \tag{3.5}$$

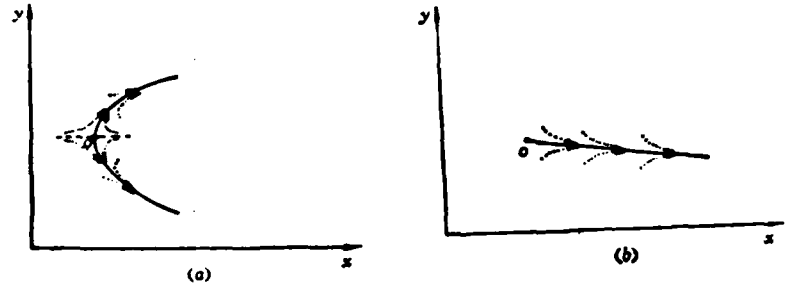

图 5　分离线的起始

Fig. 5 Origin of the separation line

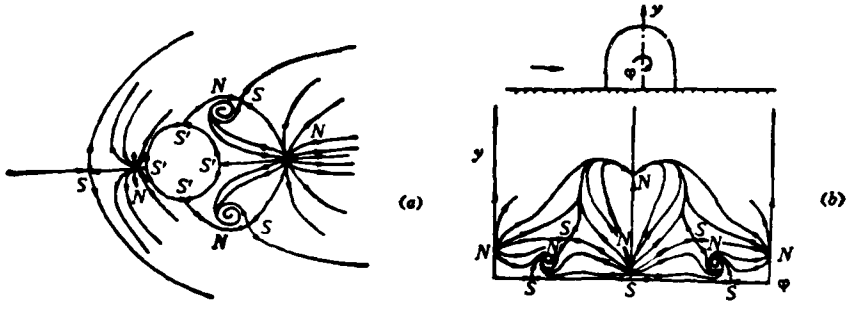

图 6　半球圆柱-平面组合体表面上的极限流线

Fig 6 Limiting streamline patterns on the hemisphere-cylinder-plane plate

where the meanings of N, S, N', and S' are the same as mentioned above. As an example, Fig.6 gives the distribution of the friction force lines and singular points of the flow around a hemisphere-cylinder erected on a surface, which is obtained by solving NS equation(48). Fig. 6(a) shows the distribution of the friction force lines and singular points on a surface. In this case, the singular point on the intersection of the cylinder and the surface is a semi-singular point. As shown in the figure, $\Sigma N = 4$. $\Sigma N' = 0$. $\Sigma S = 3$. $\Sigma S' = 4$, thus, $\left(\Sigma N + \frac{1}{2}\Sigma N'\right) - \left(\Sigma S + \frac{1}{2}\Sigma S'\right) = -1$, which satisfies topological rule (2). Fig. 6(b) is the distribution of the singular points on the hemisphere-cylinder surface. If the hemisphere-cylinder, B and the bottom surface, P are considered as an integral whole, their intersection is the tie-line of the inner points on the surface. As shown in the figure, $\Sigma N = 9$, $\Sigma S = 9$, thus, $(\Sigma N - \Sigma S)_{B+P} = 0$, which satisfies topological rule (1).

4. K. C. WANG'S METHOD AND RELATION BETWEEN TWO-DIMENSIONAL UNSTEADY FLOW AND THREE-DIMENSIONAL STEADY FLOW

According to K. C. Wang(17), if the time variable, t for two-dimensional flow is treated as a variable of space, a three-dimensional flow can be obtained. The equation describing the wall limiting streamlines for such a steady flow is

$$dx/dt = (\partial u/\partial z)_{z=0}\Delta z \qquad (4.1)$$

where z is the coordinate system perpendicular to the material surface; u, the velocity component on the wall in x direction; Δz, the step of the calculation mesh. K. C. Wang obtained the pattern of the wall limiting streamlines using equation (4.1) with the numerical solution of the boundary layer equation, and calculated the

position of the separation line (Fig. 7), based on the envelope criterion. According to K. C. Wang's method, the above-given separation conditions for two-dimensional unsteady flow and three-dimensional steady flow should be transformed from each other. This section will discuss such a transformation.

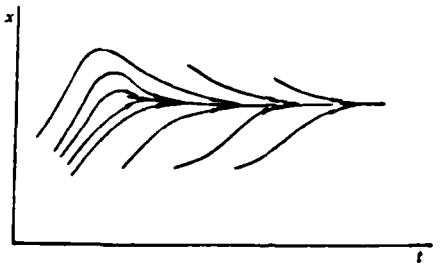

Fig. 7 Flow pattern near the separa tion line

The above coordinate system and terminology are used herein and w is assumed as the velocity component in z direction; p, as the fluid pressure; ρ, the density and ν, the dynamic viscosity, and

$$v = \frac{u_\infty}{L}\Delta z \qquad y = \left(\frac{u_\infty}{L}\, t\right)\Delta z \tag{4.2}$$

are introduced, where u_∞ is characteristic velocity of the flow field and L is the characteristic length. If pressure is a function of x only, then $\partial p/\partial t = 0$. Thus, the boundary-layer coupled equations for two-dimensional incompressible unsteady flow can be completely transformed into those for three-dimensional steady flow.

$$\begin{cases} \dfrac{\partial u}{\partial x} + \dfrac{\partial v}{\partial y} + \dfrac{\partial w}{\partial z} = 0 \\ u\dfrac{\partial u}{\partial x} + v\dfrac{\partial u}{\partial y} + w\dfrac{\partial u}{\partial z} = -\dfrac{1}{\rho}\dfrac{\partial p}{\partial x} + \nu\dfrac{\partial^2 u}{\partial z^2} \\ u\dfrac{\partial v}{\partial x} + v\dfrac{\partial v}{\partial y} + w\dfrac{\partial v}{\partial z} = -\dfrac{1}{\rho}\dfrac{\partial p}{\partial x} + \nu\dfrac{\partial^2 v}{\partial z^2} \end{cases} \tag{4.3}$$

Except that the initial condition is y=0 (t=0), the corresponding boundary-layer conditions are

$$\begin{cases} z = 0 & u = w = 0, \quad v = \dfrac{u_\infty}{L}\Delta z \\ z \to \infty & u \to u_e, \qquad v = v_e = \dfrac{u_\infty}{L}\Delta z \end{cases} \tag{4.4}$$

By transforming equation (4.2), the limiting streamline 310
equation on the wall is

$$\frac{dx}{dy} = \frac{\left(\dfrac{\partial u}{\partial z}\right)_0 \Delta z}{\dfrac{u_\infty}{L}\Delta z} = \frac{L}{u_\infty}\left(\frac{\partial u}{\partial z}\right)_0 \tag{4.5}$$

It is not difficult to verify that equation (4.5) is the same as equation (4.1).

The following discussion is based on an assumption that Δz is very small (approaches zero) and y is limited, which is equivalent to the condition where t is very large. Using the same technique in section 3 to investigate the transformed three-dimensional steady flow, the separation conditions (on the separation line) are

$$\left(\frac{\partial u}{\partial z}\right)_0 = \frac{u_\infty}{L}\operatorname{ctg}\alpha \qquad \left(\frac{\partial^2 u}{\partial z \partial \bar{x}}\sin\alpha\right)_0 < 0 \tag{4.6}$$

where $\bar{x}$ is the coordinate perpendicular to the separation line; and α is the angle between the separation line and x axis.

According to the separation conditions (4.6), we will easily obtain the pattern of the streamlines near the separation line, as shown in Fig. 7.

On the other hand, for two-dimensional unsteady flow, separation conditions (1) and (2) are given in section 2. When Δz is very small (approaches zero), it can be concluded that these two conditions are just equivalent to (4.6), and $\frac{u_\infty}{L}\operatorname{ctg}\alpha = -\frac{1}{u}\frac{\partial p}{\partial x}h$, can be obtained, where h is the distance from the separation point to the material surface. This shows that according to K. C. Wang,

the above-given separation conditions for two-dimensional unsteady flow and three-dimensional steady flow can be transformed by each other.

5. SUMMARY

This paper reviews the recent studies on the criteria for separation of two-dimensional unsteady flow and three-dimensional steady flow and the characteristic features of flow in the vicinity of the separation point and the separation line, points out the existing problems and introduces results of the author's work on the topic to date, which may be helpful in solving the existing problems.

In order to further investigate the universality of these results, it is necessary to perform numerical experiments on flows. However, the scope of the present paper is only limited to the neighbourhood of the separation point in the case of two-dimensional unsteady flow and in the vicinity of the wall separation line for three-dimensional steady flow. Since separated flows usually involve larger flow fields, it is, therefore, essential to further investigate the space structure of the separated flows. Finally, since separated flows and vortex motion are related to each other, an understanding of this relationship is of significance to engineering calculations.

[1] Moore, F. K., In boundary layer research, Proceeding of the Symposium of International Union of Theoretical and Applied Mech., H. Gorther (ed), (1957), pp.291~311.

[2] Rott, N., Quarterly Journal of Applied Mathematics, vol. 13, (1956), pp. 444~451.

[3] Sears, W. R., JAS vol. 23, (1956), pp 490~499.

[4] Sears, W. R. and Telionis, D. P., In Recent Research of Unsteady Boundary layer, E. A. Eichelbrenner (ed), vol 1, (1971), pp.404~447.

[5] Vidal, R. J., WADC, TR-59-75, (1959).

[6] Ludwig, G. R., AIAA paper 64-6, (1964).

[7] Telionis, D P and Werle, M J., JAM, vol. 95, (1973), pp.369~374.

[8] Telionis, D P, Tsahalis, D T and Werle, M J., The Physics of Fluid, vol. 17, (1973), pp. 968~973.

[9] Williams, J C. and Johnson, W D., AIAA J vol 12, (1974), pp 1388~1393.

[10] Williams, J. C., In Numerical and Physical Aspects of Aerodynamic flows, Cebeci, T. C. (ed), (1982), pp. 347～364.
[11] Wang, J. C. T. and Shen, S. F., AIAA J. vol. 16, No. 10, (1978), pp. 1025～1029.
[12] Danberg, J. E. and Fansler, K. S., AIAA J. vol. 13, No. 1, (1975), pp. 110～112.
[13] Tsahalis, D. T., AIAA J. vol. 15, No. 4, (1977), pp. 561～566.
[14] Inoue, O., AIAA J. vol. 19, No. 9, (1981), pp. 1108～1111.
[15] Dommelen, V. and Shen, S. F., Bienn. Fluid, Dyn. Symp. 13th, Olsztyn, Poland.
[16] Dommelen, V. and Shen, S. F., in Numerical and Physical Aspects of Aerodynamic flows. Cebeci, T. C. (ed), (1982), pp. 293～311.
[17] Wang, K. C., in Numerical and Physical Aspects of Aerodynamic flows, T. C. Cebeci(ed), (1982), pp. 279～291.
[18] Cebeci, T., in Numerical and Physical A Aspects of Aerodynamic flows, Cebeci, T. C. (ed), (1982), pp. 265～277.
[19] H. A. Dwyer and F. S. Sherman, in Numerical and Physical Aspects of Aerodynamic flows, T. C. Cebeci (ed), (1982), pp. 313～323.
[20] Maskell, E. C., RAE, Rep. Aero. 2565, (1955).
[21] Legendre, R., La Recherche Aeronautique, No. 54, (1956), pp. 3～8.
[22] Lighthill, M. J., in Laminar Boundary Layers, Rosenhead, L. (ed), Oxford at the Clarendon press, (1963), pp. 46～113.
[23] Oswatitsch, K., NASA TTF—15200.
[24] Wang. K. C., AIAA J. 10. (1972), pp. 1044～1050.
[25] Buckmaster, J., Phys. Fluids, 15, (1972), pp. 2106～2113.
[26] Han Taeyoung and Patel, V. C., JFM. 92, part. 4. (1979), pp. 643～657.
[27] Legendre, R., L'Aeronautique et L'Astronautique, vol. 75. No. 2, (1979), pp. 39～42.
[28] Brown, S. N. and Stewartson, K., Annual Review of Fluid Mechanics, vol. 5, (1973), pp. 339～360.
[29] Peake, D. J., NRC Canade 15471, (1976).
[30] Williams, J. C., Annual Review of Fluid Mechanics, vol. 9, (1977), pp. 113～144.
[31] Eichelbrenner, E. A. and Oudart, A., ONERA, publ. 76, Chatillon, France, (1955).
[32] Legendre, L., Rech. Aerosp. 6, (1977), pp. 327～355.
[33] Hunt, J. C. R., Abell, C. J., Peterke, J. A. and Woo, H., JFH, 86, part 1, (1978), pp. 179～200.
[34] Tobak, M. and Peake, D. J., AIAA paper 79—1480 (1979).
[35] Tobak, M. and Peake, D. J., AIAA paper 81—1260 (1981).
[36] Tobak, M. and Peake, D. J., Ann. Rev. Fluid Mechanics, vol. 14, (1982), pp. 61～85.
[37] Cousteix, J. and Houdeville, R., AIAA J. vol. 19, (1981), No8, pp. 976～985.
[38] Zhang Hanxin, Characteristics of the Three-dimensional Viscous Flow Near the Separation Line and Criteria for Separation, Proceedings, University of Science and Technology for National Defense, 82-1089(1982).

[39] Liu Moujie, Acta Aeronautica et Astronautica Sinica, Vol. 6, No. 1 (1985) pp. 1-12.

[40] Zhang Hanxin, Journal of Mechanics, 3(1983)pp. 227-232.

[41] Zhang Hanxin, Journal of Mechanics, 6(1983)pp.559-570.

[42] O' Brien, V., Phys. Fluids, 24, 6, 1981, pp. 1005~1009.

[43] Fansler, K. S. and Danberg, J. F., AIAA J. vol. 15, No.2, (1977), pp.274~276.

[44] Бам-Зеликович, Г. М., МЖГ, 2, (1970).

[45] Hirschel, E. H. and Kordulla, W., Z. Flugwiss Weltraumforsch, 4, Heft, 5, (1980), pp. 295~307.

[46] Davey, A., J. F. M. 10, (1963), pp. 593~610.

[47] Smith, J. H. B., RAE TR69119.

[48] Purohit, S. C., Shang, J. C. and Hankey, W. L., AIAA paper 82—1020, (1982).

LONGITUDINAL STABILITY ANALYSIS OF ELASTIC VEHICLES

by

Chen Shilu, Chen Xingjian, Yan Hengyuan and Huo Xiufang
(Northwestern Polytechnical University)

ABSTRACT

The longitudinal stability of elastic vehicles is studied with the effect of aeroelasticity considered. The transfer functions of an elastic vehicle with the first, second and third elastic modes taken into account are derived from the equations of its longitudinal disturbance motion. The formulas obtained can be easily used on computers and extended to cases with higher elastic modes.

The effect of aeroelasticity on the longitudinal stability of a vehicle is investigated, and a method for choosing the proper position of the gyro is proposed. Finally, the aeroelastic effect on the values of aerodynamic derivatives is estimated.

The conclusions drawn from the analysis are as follows:

(1) The aeroelastic effect on the stability of a vehicle is mainly due to the effect of the first elastic mode, while the effects of higher ones are relatively of less importance.

(2) From the viewpoint of securing stability, the gyro should be located behind the valley of the i^{th} elastic mode if the generalized force $F_{i\delta}$ and control moment M_δ for unit control deflection possess the same sign, and ahead of the valley if $F_{i\delta}$ and M_δ possess opposite signs. In the case of the investigated vehicle the gyro should be located behind the valley of the first elastic mode and ahead of the valley of the second one.

(3) The elastic aerodynamic coefficients for the investigated vehicle have values about 10～20% different from those of the corresponding rigid vehicle.

Received May 29, 1984.

NOMENCLATURE

Z_w Aerodynamic force derivative in z direction caused by the normal impact speed.

Z_q Aerodynamic force derivative in z direction caused by the angular speed of pitch.

Z_δ Aerodynamic force derivative in z direction caused by deflection of the control mechanism.

Z_{η_i} Aerodynamic force derivative in z direction caused by the generalized displacement of the ith bending mode.

$Z_{\dot{\eta}_i}$ Aerodynamic force derivative in z direction caused by the generalized displacement velocity of the ith bending mode.

ζ_i Damping coefficient of the ith bending mode structure.

F_{iq} Generalized aerodynamic force derivative of the ith bending mode in z direction caused by the angular speed of pitch.

F_{iw} Generalized aerodynamic force derivative of the ith bending mode in z direction caused by the normal impact speed.

$F_{i\delta}$ Generalized aerodynamic force derivative of the ith bending mode in z direction caused by deflection of the control mechanism.

$F_{i\eta_j}$ Generalized aerodynamic force derivative of the ith bending mode in z rirection caused by the generalized displacement of the ith bending mode.

$F_{i\dot{\eta}_j}$ Generalized aerodynamic force derivative of the ith bending mode in z direction caused by the generalized displacement velocity of the ith bending mode.

M_w Longitudinal moment derivative caused by the normal impact speed.

M_q Longitudinal moment derivative caused by the angular speed of pitch.

$M_{\dot{w}}$ Longitudinal moment derivative caused by the rate of the impact speed.

M_{η_i} Longitudinal moment derivative caused by the generalized displacement of the ith bending mode.

$M_{\dot{\eta}_i}$ Longitudinal moment derivative caused by the generalized displacement velocity of the ith bending mode.

$M_{\ddot{\eta}_i}$ Longitudinal moment derivative caused by the generalized displacement acceleration of the ith bending mode.

1. INTRODUCTION

322

In the longitudinal stability studies, some investigators[1,2] have considered an elastic vehicle as a structure where a rigid vehicle is in parallel with an elastic mode. In such a structure, however, the aerodynamic coupling effect between the rigid vehicle and the elastic mode is neglected. Other workers considered this coupling effect, but the mathematical expressions derived are complicated so that it is not feasible to conduct practical calculations.

In the present paper, the aerodynamic coupling effect between the rigid vehicle and the elastic mode is considered, and a standard matrix form of the equation of disturbance motion with parameters, such as M^*_η and M^*_δ, is presented, which makes it feasible to use the standard compute code during calculation. Compared with those introduced in literature [3-6], this technique has the potential to consider higher elastic modes.

The effect of gyro location on elastic vehicle stability is analyzed together with the coupling effects of the elastic mode and the control system. It is believed that the suitability of the gyro location is related to the same sign of the generalized force, $F_{i\delta}$ and the control moment, M_δ. Results of universal significance are given. The effect of aeroelasticity on aerodynamic force derivatives for a rigid vehicle is also discussed.

2. EQUATIONS OF ELASTIC VEHICLE LONGITUDINAL DISTURBANCE MOTION

Now we are going to establish equations of the short-period vehicle longitudinal disturbance motion with aeroelasticity taken into account.

The aerodynamic force and moment are related to the local angle of attack, $\alpha(x, y, t)$ or the local impact speed, $w(x, y, t)=u_0\alpha(x, y, t)$, , and the local angular speed of pitch, $\dot{\vartheta}(x, y, t)$.

Let us assume x, y, z as the coordinates in the average body axis whose origin is the instantaneous center of mass, and express elastic deformation as $\xi(x, y, t)=\sum_{i=1}^{n}\phi_i(x, y)\eta_i(t)$, , where $\phi_i(x, y)$ is mode function, and $\eta_i(t)$ is the generalized coordinate.

The equations of the nth mode short-period small perturbation can be expressed as

$$\dot{w}(t)-U_0\dot{\vartheta}(t)=\int_y\int_x\frac{\partial^2 Z_w}{\partial x\partial y}w(x, y, t)dxdy+\int_y\int_x\frac{\partial^2 Z_q}{\partial x\partial y}\dot{\vartheta}(x, y, t)dxdy+Z_\delta\delta(t) \tag{2.1a}$$

$$\ddot{\vartheta}(t)=\int_y\int_x\frac{\partial^2 M_w}{\partial x\partial y}w(x, y, t)dxdy+\int_y\int_x\frac{\partial^2 M_{\dot{w}}}{\partial x\partial y}\dot{w}(x, y, t)dxdy+\int_y\int_x\frac{\partial^2 M_q}{\partial x\partial y}\dot{\vartheta}(x, y, t)dxdy+M_\delta\delta(t) \tag{2.1b}$$

$$\ddot{\eta}_i(t)+2\zeta_i\omega_i\dot{\eta}_i(t)+\omega_i^2\eta_i(t)=\frac{Q_i(t)}{m_i(t)} \tag{2.1c}$$

where $Q_i(t)$ is the generalized force, and $m_i(t)$ is the generalized mass. They can be expressed as

$$Q_i(t)=\int_y\int_x \frac{\partial^2 Z(t)}{\partial x\partial y}\phi_i(x,\ y)dxdy \tag{2.2a}$$

$$m_i(t)=\int_y\int_x m(x,\ y)[\phi_i(x,\ y)]^2dxdy \tag{2.2b}$$

The integral terms and the generalized force term in eqns. (2.1) are functions of w(x,y,t) and $\dot{\vartheta}(z,y,t)$. When aeroelasticity is taken into account, the latter two functions should be 323

$$w(x,\ y,\ t)=w(t)+\sum_{i=1}^{n}\phi_i(x,\ y)\eta_i(t)-\sum_{i=1}^{n}u_0\phi_i'(x,\ y)\eta_i(t) \tag{2.3a}$$

$$q=\dot{\vartheta}(x,\ y,\ t)=\dot{\vartheta}(t)-\sum_{i=1}^{n}\phi_i'(x,\ y)\dot{\eta}_i(t) \tag{2.3b}$$

where $(\dot{})$ denotes a derivative with respect to t, and $(')$, that with respect to x. Substituting the values of $w(x,y,t)$, $\dot{\vartheta}(x,\ y,\ t)$ and rearranging them, equations of the elastic vehicle longitudinal disturbance are obtained:

$$\dot{w}(t)-u_0\dot{\vartheta}(t)=Z_w\cdot w(t)+Z_\vartheta\vartheta(t)+\sum_{i=1}^{n}[Z_{\eta_i}\eta_i(t)+Z_{\dot{\eta}_i}\dot{\eta}_i(t)]+Z_\delta\delta(t) \tag{2.4a}$$

$$\ddot{\vartheta}(t)=M_w\dot{w}(t)+M_w w(t)+M_\vartheta\vartheta(t)+\sum_{i=1}^{n}[M_{\eta_i}\eta_i(t)+M_{\dot{\eta}_i}\dot{\eta}_i(t)+M_{\ddot{\eta}_i}\ddot{\eta}_i(t)]+M_\delta\delta(t) \tag{2.4b}$$

$$\ddot{\eta}(t)+2\zeta_i\omega_i\dot{\eta}_i(t)+\omega_i^2\eta_i(t)=F_{iw}W(t)+F_{i\vartheta}\vartheta(t)+\sum_{i=1}^{n}[F_{i\eta_j}\eta_j(t)+F_{i\dot{\eta}_j}\dot{\eta}_i(t)]+F_{i\delta}\delta(t) \tag{2.4c}$$

where Z_{η_i}, $Z_{\dot{\eta}_i}$, M_{η_i}, $M_{\dot{\eta}_i}$, $M_{\ddot{\eta}_i}$, F_{iw}, $F_{i\vartheta}$, $F_{i\eta_j}$, $F_{i\dot{\eta}_j}$, $F_{i\delta}$ are coefficients relating to the elastic modes:

$$Z_{\eta_i} = -u_0 \int_y \int_x \frac{\partial^2 Z_w}{\partial x \partial y} \phi_i'(x, y)\,dxdy \tag{2.5}$$

$$Z_{\dot{q}_i} = \int_y \int_x \frac{\partial^2 Z_w}{\partial x \partial y} \phi_i(x, y)\,dxdy - \int_y \int_x \frac{\partial^2 Z_q}{\partial x \partial y} \phi_i'(x, y)\,dxdy \tag{2.6}$$

$$M_{\eta_i} = -u_0 \int_y \int_x \frac{\partial^2 M_w}{\partial x \partial y} \phi_i'(x, y)\,dxdy \tag{2.7}$$

$$M_{\dot{q}_i} = \int_y \int_x \left\{ \frac{\partial^2 M_w}{\partial x \partial y} \phi_i(x, y) - \left[u_0 \frac{\partial^2 M_{\dot{w}}}{\partial x \partial y} + \frac{\partial^2 M_q}{\partial x \partial y} \right] \phi_i'(x, y) \right\} dxdy \tag{2.8}$$

$$M_{\ddot{q}_i} = \int_y \int_x \frac{\partial^2 M_{\dot{w}}}{\partial x \partial y} \phi_i(x, y)\,dxdy \tag{2.9}$$

$$F_{iw} = \frac{M}{m_i} \int_y \int_x \frac{\partial^2 Z_w}{\partial x \partial y} \phi_i(x, y)\,dxdy \tag{2.10}$$

$$F_{iq} = \frac{M}{m_i} \int_y \int_x \frac{\partial^2 Z_q}{\partial x \partial y} \phi_i(x, y)\,dxdy \tag{2.11}$$

$$F_{i\eta_j} = \frac{-u_0 M}{m_i} \int_y \int_x \frac{\partial^2 Z_w}{\partial x \partial y} \phi_i(x, y) \phi_j'(x, y)\,dxdy \tag{2.12}$$

$$F_{i\dot{q}_j} = \frac{M}{m_i} \int_y \int_x \left[\frac{\partial^2 Z_w}{\partial x \partial y} \phi_i(x, y) \phi_j(x, y) - \frac{\partial^2 Z_q}{\partial x \partial y} \phi_i(x, y) \phi_j'(x, y) \right] dxdy \tag{2.13}$$

$$F_{ib} = \frac{M}{m_i} \int_y \int_x \frac{\partial^2 Z_b}{\partial x \partial y} \phi_i(x, y)\,dxdy \tag{2.14}$$

3. CALCULATION OF ELASTIC VEHICLE TRANSFER FUNCTIONS TAKING INTO ACCOUNT THE FIRST, SECOND AND THIRD MODES

In order to make the calculation easier, Laplacian transform was conducted for eqns (2.4) to get a standard matrix form, so that the matrix compute code can be used in this calculation.

Let us assume the third vibration mode. Then, the matrix form of the coupled linear equations is obtained as follows:

$$
\begin{bmatrix}
Z_w - s & u_0 + Z_q & 0 & Z_{\dot{\eta}_1} & Z_{\eta_1} & Z_{\dot{\eta}_2} \\
M^*_w & M^*_q - s & 0 & M^*_{\dot{\eta}_1} & M^*_{\eta_1} & M^*_{\dot{\eta}_2} \\
0 & 1 & -s & 0 & 0 & 0 \\
F_{1w} & F_{1q} & 0 & (F_{1\dot{\eta}_1} - 2\zeta_1\omega_1 - s) & (F_{1\eta_1} - \omega_1^2) & F_{1\dot{\eta}_2} \\
0 & 0 & 0 & 1 & -s & 0 \\
F_{2w} & F_{2q} & 0 & F_{2\dot{\eta}_1} & F_{2\eta_1} & (F_{2\dot{\eta}_2} - 2\zeta_2\omega_2 - s) \\
0 & 0 & 0 & 0 & 0 & 1 \\
F_{3w} & F_{3q} & 0 & F_{3\dot{\eta}_1} & F_{3\eta_1} & F_{3\dot{\eta}_2} \\
0 & 0 & 0 & 0 & 0 & 0
\end{bmatrix}
$$

$$
\begin{bmatrix}
Z_{\eta_2} & Z_{\dot{\eta}_3} & Z_{\eta_3} \\
M^*_{\eta_2} & M^*_{\dot{\eta}_3} & M^*_{\eta_3} \\
0 & 0 & 0 \\
F_{1\eta_2} & F_{1\dot{\eta}_3} & F_{1\eta_3} \\
0 & 0 & 0 \\
F_{2\eta_2} - \omega_2^2 & F_{2\dot{\eta}_3} & F_{2\eta_3} \\
-s & 0 & 0 \\
F_{3\eta_2} & (F_{3\dot{\eta}_3} - 2\zeta_3\omega_3 - s) & (F_{3\eta_3} - \omega_3^2) \\
0 & 1 & -s
\end{bmatrix}
\begin{bmatrix}
w(s) \\ \dot{\vartheta}(s) \\ \vartheta(s) \\ \dot{\eta}_1(s) \\ \eta_1(s) \\ \dot{\eta}_2(s) \\ \eta_2(s) \\ \dot{\eta}_3(s) \\ \eta_3(s)
\end{bmatrix}
=
\begin{bmatrix}
-Z_\delta \\ -M^*_\delta \\ 0 \\ -F_{1\delta} \\ 0 \\ -F_{2\delta} \\ 0 \\ -F_{3\delta} \\ 0
\end{bmatrix}
\delta(s) \qquad (3.1)
$$

where

$$
\left.
\begin{aligned}
M^*_w &= M_w + M_{\dot{w}} Z_w + M_{\dot{\eta}_1} F_{1w} + M_{\dot{\eta}_2} F_{2w} + M_{\dot{\eta}_3} F_{3w} \\
M^*_q &= M_q + M_{\dot{w}} (u_0 + Z_q) + M_{\dot{\eta}_1} F_{1q} + M_{\dot{\eta}_2} F_{2q} + M_{\dot{\eta}_3} F_{3q} \\
M^*_{\dot{\eta}_1} &= M_{\dot{\eta}_1} + M_{\dot{w}} Z_{\dot{\eta}_1} + M_{\dot{\eta}_1} (F_{1\dot{\eta}_1} - 2\zeta_1\omega_1) + M_{\dot{\eta}_2} F_{2\dot{\eta}_1} + M_{\dot{\eta}_3} F_{3\dot{\eta}_1} \\
M^*_{\eta_1} &= M_{\eta_1} + M_{\dot{w}} Z_{\eta_1} + M_{\dot{\eta}_1} (F_{1\eta_1} - \omega_1^2) + M_{\dot{\eta}_2} F_{2\eta_1} + M_{\dot{\eta}_3} F_{3\eta_1} \\
M^*_{\dot{\eta}_2} &= M_{\dot{\eta}_2} + M_{\dot{w}} Z_{\dot{\eta}_2} + M_{\dot{\eta}_1} F_{1\dot{\eta}_2} + M_{\dot{\eta}_2} (F_{2\dot{\eta}_2} - 2\zeta_2\omega_2) + M_{\dot{\eta}_3} F_{3\dot{\eta}_2} \\
M^*_{\eta_2} &= M_{\eta_2} + M_{\dot{w}} Z_{\eta_2} + M_{\dot{\eta}_1} F_{1\eta_2} + M_{\dot{\eta}_2} (F_{2\eta_2} - \omega_2^2) + M_{\dot{\eta}_3} F_{3\eta_2} \\
M^*_{\dot{\eta}_3} &= M_{\dot{\eta}_3} + M_{\dot{w}} Z_{\dot{\eta}_3} + M_{\dot{\eta}_1} F_{1\dot{\eta}_3} + M_{\dot{\eta}_2} F_{2\dot{\eta}_3} + M_{\dot{\eta}_3} (F_{3\dot{\eta}_3} - 2\zeta_3\omega_3) \\
M^*_{\eta_3} &= M_{\eta_3} + M_{\dot{w}} Z_{\eta_3} + M_{\dot{\eta}_1} F_{1\eta_3} + M_{\dot{\eta}_2} F_{2\eta_3} + M_{\dot{\eta}_3} (F_{3\eta_3} - \omega_3^2) \\
M^*_\delta &= M_\delta + M_{\dot{w}} Z_\delta + M_{\dot{\eta}_1} F_{1\delta} + M_{\dot{\eta}_2} F_{2\delta} + M_{\dot{\eta}_3} F_{3\delta}
\end{aligned}
\right\} \qquad (3.2)
$$

When higher vibration modes are considered, the same method can be used. From eqn. (3.1), we have the transfer functions:

$$
W_\vartheta(s) = \frac{\Delta_\vartheta}{\Delta} = \frac{c_0 s^7 + c_1 s^6 + c_2 s^5 + c_3 s^4 + c_4 s^3 + c_5 s^2 + c_6 s + c_7}{s\,(s^8 + a_1 s^7 + a_2 s^6 + a_3 s^5 + a_4 s^4 + a_5 s^3 + a_6 s^2 + a_7 s + a_8)} \qquad (3.3)
$$

$$W_{\eta 1}(s)=\frac{\Delta_{\eta 1}}{\Delta}=\frac{d_{10}s^7+d_{11}s^6+d_{12}s^5+d_{13}s^4+d_{14}s^3+d_{15}s^2+d_{16}s+d_{17}}{s\,(s^8+a_1s^7+a_2s^6+a_3s^5+a_4s^4+a_5s^3+a_6s^2+a_7s+a_8)} \tag{3.4}$$

$$W_{\eta 2}(s)=\frac{\Delta_{\eta 2}}{\Delta}=\frac{d_{20}s^7+d_{21}s^6+d_{22}s^5+d_{23}s^4+d_{24}s^3+d_{25}s^2+d_{26}s+d_{27}}{s\,(s^8+a_1s^7+a_2s^6+a_3s^5+a_4s^4+a_5s^3+a_6s^2+a_7s+a_8)} \tag{3.5}$$

$$W_{\eta 3}(s)=\frac{\Delta_{\eta 3}}{\Delta}=\frac{d_{30}s^7+d_{31}s^6+d_{32}s^5+d_{33}s^4+d_{34}s^3+d_{35}s^2+d_{36}s+d_{37}}{s\,(s^8+a_1s^7+a_2s^6+a_3s^5+a_4s^4+a_5s^3+a_6s^2+a_7s+a_8)} \tag{3.6}$$

where $d_{17}=d_{27}=d_{37}=0$, and $b_0=M_\delta$, $d_{10}=F_{1\delta}$, $d_{20}=F_{2\delta}$, $d_{30}=F_{3\delta}$.

In the case of a closed-ring system, the angle to which the gyro is subjected contains not only ϑ, but also the partial deflection angle resulted from various modes at the point. Thus, the gyro-subjected angle ϑ_l is

$$\vartheta_l=\vartheta+[-\varphi_1'(l)]\eta_1+[-\varphi_2'(l)]\eta_2+[-\varphi_3'(l)]\eta_3 \tag{3.7}$$

where $\varphi_1'(l)$, $\varphi_2'(l)$, $\varphi_3'(l)$ are derivatives of various vibration modes of the gyro at point 1 with respect to x. Then, transfer function, $W_{\vartheta l}(s)$ is

$$\begin{aligned}W_{\vartheta l}(s)&=W_\vartheta-\varphi_1'(l)W_{\eta_1}(s)-\varphi_2'(l)W_{\eta_2}(s)-\varphi_3'(l)W_{\eta_3}(s)\\&=\frac{l_0s^7+l_1s^6+l_2s^5+l_3s^4+l_4s^3+l_5s^2+l_6s+l_7}{s\,(s^8+a_1s^7+a_2s^6+a_3s^5+a_4s^4+a_5s^3+a_6s^2+a_7s+a_8)}\end{aligned} \tag{3.8}$$

where the coefficients of the terms in the numerator are

$$l_i=c_i-\varphi_1'(l)d_{1i}-\varphi_2'(l)d_{2i}-\varphi_3'(l)d_{3i}\quad i=0\sim 7 \tag{3.9}$$

It can be shown that in a closed-ring system, $W_{\vartheta l}$ and W_δ have the same nominator but different numerators. When the root locus method is used, as we will discuss shortly, the extreme points of $W_{\vartheta l}$ and W_δ are the same, but the zero point distributions are different. Results of the sample calculation selected in this paper are shown in Table 1.

Table 1. Roots of the determinants

Δ	0	$-3.546 \pm 34.777\,i$	$-4.584 \pm 321.192\,i$	$-31.471 \pm 761.227\,i$	$-20.646 \pm 1177.87\,i$
Δ_θ	-13.51	—	$-14.909 \pm 288.396\,i$	$-42.790 \pm 749.657\,i$	$-18.499 \pm 1179.50\,i$
Δ_n	0	$-3.675 \pm 34.354\,i$	—	$-31.444 \pm 759.876\,i$	$-20.652 \pm 1178.08\,i$
Δ_{n_2}	0	$-3.841 \pm 33.797\,i$	$-3.327 \pm 317.153\,i$	—	$-20.708 \pm 1178.11\,i$
Δ_{n_3}	0	$-1.887 \pm 33.778\,i$	$-5.390 \pm 321.387\,i$	$-31.701 \pm 761.058\,i$	—

4. EFFECT OF ELASTIC BODY ON THE CLOSE-RING SYSTEM STABILITY

The stability of a closed-ring system can be discussed in terms of the distribution of the zero points and extreme points, and their changes in an open-ring system. In this section, only changes in the zero extreme points of an elastic body will be discussed. It is assumed that the gyro and the automatic machine are ideal proportional links.

As mentioned above, having considered the effect of the partial deflection, $W_{\vartheta l_0}$, which is given by eqn. (3.8), is used as the elastic body transfer function in the closed-ring system. This function has exactly the same nominator as W_ϑ in eqn. (3.3). It is independent upon the location of the gyro.

The coefficients of various terms of the numerator in eqn. (3.8) are determined by eqn. (3.9) where the coefficients c_i, d_{1i}, d_{2i}, d_{3i} are influenced by aerodynamic coupling. It is more important that $\varphi_1'(l)$, $\varphi_2'(l)$, $\varphi_3'(l)$, are closely related to the gyro location and may have opposite signs at different points. Thus, selection of different l (the gyro location) has appreciable influence on coef-

ficients, l_0-l_7.

It is shown from the sample calculation that coefficients c_i are all positive. Although d_{1i}, d_{2i} and d_{3i} can assume either positive or negative values, the corresponding coefficients for the same vibration mode have the same sign, since every mode itself is stable.

If one point is found to make the last three terms on the right side of eqn. (3.9)

$$-\varphi_1'(l)d_{1i}-\varphi_2'(l)d_{2i}-\varphi_3'(l)d_{3i}=0$$

then, $W_{\vartheta l}$ is equal to W_{ϑ}. This means that the elastic vibration effect is completely vanished. It is, however, very difficult to determine this point accurately. A suitable region should be given here, e.g., $\{-\varphi_1'(l)d_{1i}-\varphi_2'(l)d_{2i}-\varphi_3'(l)d_{3i}\}>0$. For instance, a point is chosen where $\varphi_1'(l)=-0.24,\ \varphi_2'(l)=0.195,\ \varphi_3'(l)=-0.46$, then, $-\varphi_1'(l)d_{1i}-\varphi_2'(l)d_{2i}-\varphi_3'(l)d_{3i}>0$. Also, when $i=0\sim6$, $l_i>c_i>0$ (see Table 2) and $l_7=c_7=0.1460\times10^{21}$.

The zero points determined by coefficients, l_i are

$$-9.161,\ -1.856\pm136.6i,\ -19.17\pm595.8i,\ -20.22\pm1271i$$

Compared with the corresponding zero points of Δ_ϑ in Table 1, except that the last pair of zero points slightly moved left, all the others moved considerably right. The last pair have only slight influence on stability due to the coupled pair formation with corresponding extreme point.

Since c_i has the same sign as M_ϑ, the signs of d_{1i}, d_{2i} and d_{3i} are the same as those of $F_{1\vartheta}$, $F_{2\vartheta}$, and $F_{3\vartheta}$, respectively. In order for $-\{\varphi_1'(l)d_{1i}+\varphi_2'(l)d_{2i}+\varphi_3'(l)d_{3i}\}$ and c_i to have the same sign, the gyro should be located slightly behind the valley of the ith

vibration mode; conversely, it should be located slightly ahead of the valley. In the case of the sample calculation described in this paper, the gyro may be located behind the valley of the first mode, but ahead of that of the second one. Since the third mode has slight influence ($|d_{3i}|$ is small), it was not taken into account.

5. ESTIMATION OF THE EFFECT OF ELASTIC VIBRATION ON AERODYNAMIC FORCE AND MOMENTS

From eqn. (2.4) and the aerodynamic derivatives of a rigid body, the following relations can be obtained (where subscript, e denotes elastic body, and r, rigid body):

$$\frac{(c_L^a)_e}{(c_L^a)_r} = 1 + \frac{1}{c_L^a \alpha} \sum_{i=1}^{n} \bar{c}_{L_i}^a \left(-\phi_i' \eta_i + \phi_i \frac{\dot{\eta}_i}{u_0} \right) \tag{5.1}$$

$$\frac{(c_L^m)_e}{(c_L^m)_r} = 1 - \sum_{i=1}^{n} \frac{\bar{c}_{L_i}^m \phi_i'}{c_L^m \omega} \cdot \dot{\eta}_i \tag{5.2}$$

$$\frac{(c_m^a)_e}{(c_m^a)_r} = 1 + \sum_{i=1}^{n} \frac{\bar{c}_{m_i}^a}{c_m^a \alpha} \left(-\phi_i' \eta_i + \phi_i \frac{\dot{\eta}_i}{u_0} \right) \tag{5.3}$$

$$\frac{(c_m^{\dot{a}})_e}{(c_m^{\dot{a}})_r} = 1 + \sum_{i=1}^{n} \frac{\bar{c}_{m_i}^{\dot{a}}}{c_m^{\dot{a}} \dot{\alpha}} \left(-\phi_i' \dot{\eta}_i + \phi_i \frac{\ddot{\eta}_i}{u_0} \right) \tag{5.4}$$

$$\frac{(c_m^m)_e}{(c_m^m)_r} = 1 + \sum_{i=1}^{n} \frac{\bar{c}_{m_i}^m}{c_m^m \omega} (-\phi_i' \dot{\eta}_i) \tag{5.5}$$

where the aerodynamic derivatives with bars (e.g., $\bar{c}_{L_i}^a$, $\bar{c}_{L_i}^m \cdots$) stand for the means of the aerodynamic derivatives in various integral intervals, respectively, i.e.,

$$\bar{c}^{a}_{L_i}=\frac{s_i}{s}\iint_{s_i}\frac{\partial^2 c^{a}_{L}}{\partial x\partial y}\,dxdy,\quad \bar{c}^{a}_{L_i}=\frac{s_i}{s}$$
$$\times\iint_{s_i}\frac{\partial^2 c^{w}_{L}}{\partial x\partial y}dxdy,\ \bar{c}^{a}_{m_i}=\frac{s_i}{s}\iint_{s_i}\frac{\partial^2 c^{a}_{m}}{\partial x\partial y}\,dxdy, \tag{5.6}$$
$$\bar{c}^{\dot{a}}_{m_i}=\frac{s_i}{s}\iint_{s_i}\frac{\partial^2 c^{\dot{a}}_{m}}{\partial x\partial y}\,dxdy,\quad \bar{c}^{w}_{m_i}=\frac{s_i}{s}$$
$$\times\iint_{s_i}\frac{\partial^2 c^{w}_{m}}{\partial x\partial y}dxdy$$

In this example with elastic vibrations taken into account, the aerodynamic derivatives are 10-20% different from those of rigid vehicles (see Fig. 1)

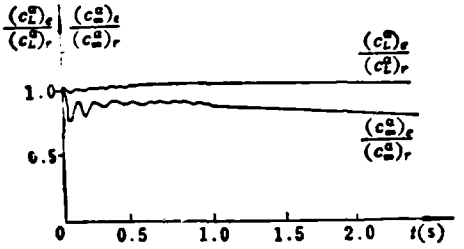

图 1 $\frac{(c^{a}_{L})_e}{(c^{a}_{L})_r}$和$\frac{(c^{a}_{m})_e}{(c^{a}_{m})_r}$的过渡过程

Fig 1 Transient process of $\frac{(c^{a}_{L})_e}{(c^{a}_{L})_r}$ and $\frac{(c^{a}_{m})_e}{(c^{a}_{m})_r}$

6. CONCLUSIONS

Based on the above discussion, we can conclude that

(1) When the effect of aeroelasticity on vehicle motion is considered, we can draw a conclusion which agrees with the characteristic features of the common vehicles in small and medium sizes: the effect of the first elastic mode on the vehicle stability is significant while that of higher ones are not.

(2) In order to avoid elastic vibrations lowering the stability of the overall missile system, the gyro should be located behind the valley of the ith elastic mode if $F_{i\delta}$ and M_δ have the same sign, and ahead of the valley if $F_{i\delta}$ and M_δ assume the opposite signs. This is a conclusion of universal significance. In the case of the sample calculation, the gyro should be located behind the valley of the first elastic mode and ahead of the valley of the second one.

(3) Using the theoretical expression established in this work for the ratio of the aerodynamic coefficient of an elastic vehicle to that of a rigid one, the sample calculation shows that the elastic aerodynamic coefficients are 10-20% different from those of the corresponding rigid vehicle.

REFERENCES

[1] Shatalov, A.S., Aerospace Vehicles as Object of Control, NASA TT F-809, (1974), pp. 120~129.

[2] Greensite, A., Analysis and Design of Space Vehicle Flight Contol Systems, Sparton Books, New York, (1970), pp. 305~310.

[3] Roskam, J and Dusto, A., A Method for Predicting Longitudinal Stability Derivative of Rigid and Elastic Airplane, Journal of Aircraft, Vol. 6, (1969), pp. 525~531.

[4] K. C. (Names not given) et al., Translated by Guan Shiyi, et al., Elastic Vehicles as Objects of Automatic Control, Publishing House of National Defense Industry, pp. 154-158 and pp. 166-170(1979).

[5] Swaim *R. L.* and Fullman, *D. G.*, Prediction of Elastic Airplane Longitudinal Dynamics from Rigid-Body Aerodynamics, Journal of Aircraft, Vol. 14, No. 9, (1977), pp. 868~874

[6] Swaim *R. L.* and Fullman, *D. G.*, Prediction of Elastic Airplane Lateral Dynamics from Rigid-Body Aerodynamics, Journal of Aircraft, Vol. 15, No. 9, 1978, pp. 392~398.

A VORTEX LATTICE METHOD FOR JET WING PERFORMANCE WITH NONLINEAR WAKE AND TIP FLOW

by

Chen Zelin
(Beijing Institute of Aerodynamics)

and

J. M. Wu
(University of Tennessee Space Institute)

ABSTRACT

A three-dimensional nonlinear method for determining the aerodynamic performance of a jet flap wing has been developed. The method utilizes a system of bound and free vortices with vortex lattices to represent the wing, jetwake and tip vortices. The kinematic boundary conditions are satisfied at the wing, as the ordinary vortex lattice theory states. But the feature of the present method lies in satisfaction of both kinematic and dynamic conditions and consideration of vortex interaction. The solutions obtained include chordwise and spanwise load distributions, from which sectional and total aerodynamic quantities are derived. In the solution the jet-wake sheet and the tip vortex shape are determined simultaneously with the nonlinear effects taken into account. The solutions obtained by the present method agree well with other analytical results and available data for a jet wing with large aspect ratio. The present method has no limitation on the aspect ratio and is applicable to the cases with large jet blowing angles as well. The partial span jet blowing and the disturbance of main wing blowing to the second wing are also treated in this paper.

Received March 21, 1984.

1. INTRODUCTION

It is a well-known principle to produce strong lift by using jet-flapped wings (JFWs). Application of such wings pushes forward their aerodynamic performance studies. In two-dimensions, Spence[1] has established the JFW shape theory, which states that when the jet thickness tends towards zero, the jet momentum is still kept a limited value while the jet mass flow rate tends towards zero. Spence's hypothesis has been accepted by most investigators. In cases where the jet structure and viscous effect need not to be considered, this hypothesis agrees approximately with the actual JFW's physical properties, and usually gives good results. The two representative methods which can be taken as examples are Halsey's elementary vortex distribution and Sato's conformed map. In three-dimensional cases, various methods based on lifting-line and lifting-surface theories, such as those proposed by Maskell and Spence,[4] Las,[5] Shen and Lopez, and Wasson, have been developed. The elementary vortex distribution method given in literature[6] is based on the linearization theory, and the boundary layer conditions for the wing and jet are satisfied over a given surface. Calculation results for large aspect-ratio wings using this method agree well with experimental data. In the case of small aspect-ratio wings or large jet blowing angles, however, the nonlinear effects should be taken into account.

Big progress in the vortex lattice theory for determining aerodynamic performance of wings has been made recently,[7-9] and several methods have been developed to solve problems caused by a vortex singularity. Among these methods is the concept of so-

called "limited-nuclear vortex". Nevertheless, further investigation is needed, since utilization of the vortex nuclear's empirical data may lead to a decrease of calculation accuracy.

In the present investigation, the vortex lattice method was used in the JFW's study. The wing, jet, wake and tip vortices were represented by vortices. The kinematic and dynamic conditions were satisfied at the wing and the jet surface. The shapes of the jet, wake and tip vortices were simultaneously obtained as part of the solution with the nonlinear effects taken into account. The present method has no limitation on the aspect ratio and the jet blowing angle, and is applicable to wings with any shapes of surface, cross-section, and jet momentum distributions.

2. METHOD AND BOUNDARY CONDITIONS

230

Let us use the hypothesis of an incompressible potential flow without taking separation and viscous effects into account, and use Laplacian equation

$$\nabla^2\phi = 0 \qquad (1)$$

where ϕ is the velocity potential. The solution is expressed as a vortex lattice which satisfies this equation.

The boundary layer conditions required by equation (1) can be divided into kinematic and dynamic conditions. The kinematic condition is that the air flow is tangential to the material surface. If the jet location is known, the air flow can be taken as the material surface and the kinematic condition has been satisfied. In addition, the jet should satisfy the dynamic condition that the pressure difference, to which the jet is subjected, p is

in equilibrium with the centrifugal force

$$\Delta p = -j/r \tag{2}$$

where j is the jet flow rate in unit span; and r is the partial curvature radius of the jet. Based on Spence's hypothesis,[1] eqn. (2) can be written as

$$\gamma\bar{v} = cC_\mu/2r \tag{3}$$

where γ is the vortex intensity; $\bar{v}$, mean of the velocities above and beneath the jet surface; c, the chord length of the wing; and $C\mu$, the jet momentum coefficient.

Let us use the Kutta's conditions to make the solution unique. In the absence of the jet, these conditions are satisfied at the back fringe. In the presence of the jet, the jet at far lower reach needs to be parallel to the freestream flow direction. In addition, it is assumed that there is no transverse momentum transfer within the jet, i.e., the momentum is kept constant along a jet vortex line. This hypothesis appears fairly reasonable when the spanwise variation of the $C\mu$ distribution is not appreciable.

It is shown that the JFW lifting surface theory presented in this paper is different from other common theories in mixed boundary layer conditions and unknown jet location, which makes the equation solving more difficult.

3. SOLVING PROCESS

Vortices were used to represent the wing, wake, the tip vortices and the jet surface (Fig. 1). Here, the wing was devided into several surface elements, each being expressed by a hoof vortex. The bound vortices were on the wing and the free vortices constructed

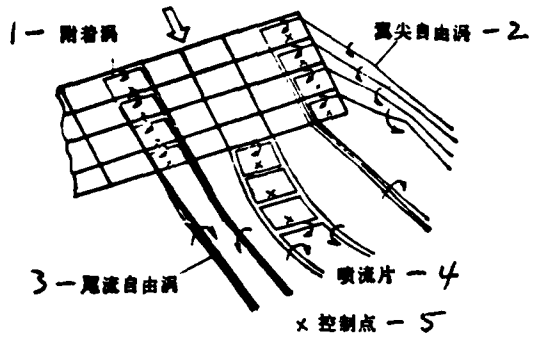

图 1 奇点分布示意图

Fig. 1 Sketch of singular point distribution

1-bound vortex; 2-free tip vortex; 3-free wake vortex; 4-jet sheet; and 5-control point.

the wake and the tip vortices. The spanwise bound vortices were located at $\frac{1}{4}$ chord length of the corresponding surface elements and the control points at 3/4 chord length. Wherever a jet existed, the wake was neglected. The jet was expressed by a vortex lattice system, the control points of which were located at 3/4 chord length. The thickness effect was not considered in this calculation.

Since the locations of the jet, wake and tip vortices were unknowns, iteration solving methods were used. Basically, there are two iteration methods: (1) Start with a jet shape which satisfies the kinematic condition, and then find the jet shape which simultaneously satisfies both dynamic and kinematic conditions; and (2) Begin with a jet shape which satisfies the dynamic condition, and then find one which satisfies simultaneously both conditions. Halsey has pointed out that the first is not a dependable method and it is difficult to get a convergence from this method. Our results have already shown this disadvantage. This is the reason why we chose the second method in this study.

331

During calculation, we utilized a method in which the coefficients were to be determined to find the jet shape.[11] Results show that introduction of suitable functions can speed up the iteration process. It is believed that the functions to be se-

lected are not unique and functions in different forms can be used to express the jet shape in defferent problems.

4. RESULTS AND DISCUSSION

Calculations were performed for typical JFWs in this investigation. The calculation conditions are shown in Figs. 2-4. Figs. 2 and 3 give the spanwise distribution of the normal force and the chordwise distribution of pressure at half wing span. The data obtained are 10% higher than those given in literature [6], especially for the front and back fringes. Further study is needed to find the reason for this difference. One of the reason is probably neglect of considering the wake at the location where there is a jet, namely, neglect of the controlling effect of the wake on the jet, resulting in higher calculation values of the normal force. Fig. 4 gives Das' experimental results which are in between the calculation values given in this paper and those in literature [6]. Fig. 6 gives results on partial span jet blowing. Neglecting the wake at the jet and its vicinity, a simplified inviscid model results. Fig. 6 shows the calculation results for the combination of the wing and the tail, indicating that the influence of the main wing jet on the tip vortices of the second wing (tail) did not fully developed. Results for the case of a large jet-blowing angle and a small aspect ratio are given in Figs. 7 and 8, which show the calculation capability of this method.

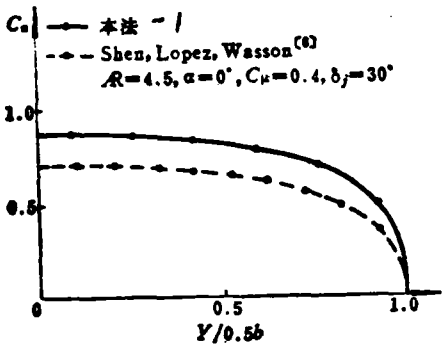

图 2　法向力系数展向分布

Fig. 2 Spanwise distribution of normal force coefficient

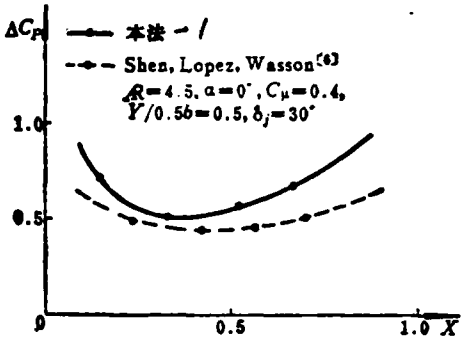

图 3　压力系数弦向分布（α = 0°）

Fig. 3 Chordwise distribution of preseure coefficient（α = 0°）

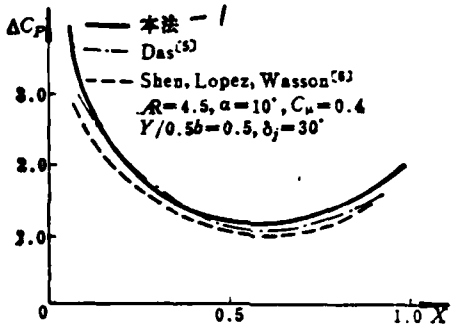

图 4　压力系数弦向分布（α = 10°）

Fig. 4 Chordwise distribution of pressure coefficient（α = 10°）

1-this method.

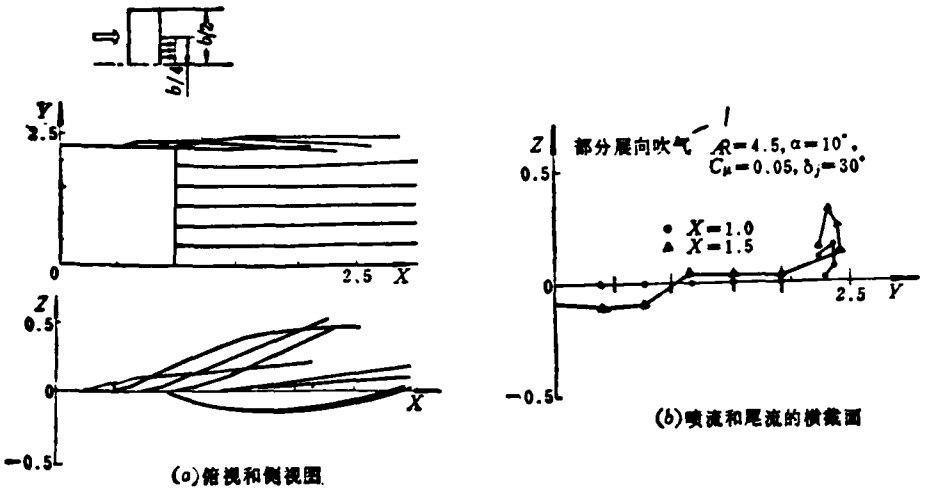

Fig. 5 The shape of jet and wake on partial span jet blowing
(*a*) vertical and side view; (*b*) cross-section.

1-partial span blowing.

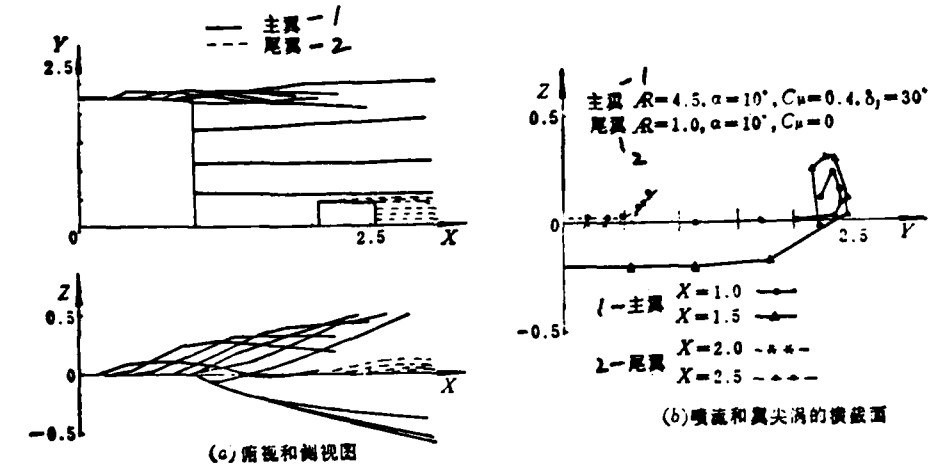

Fig 6 Interference of main wing jet on tail
(*a*) vertical and side view; (*b*) cross-section.

1-main wing; and 2-tail.

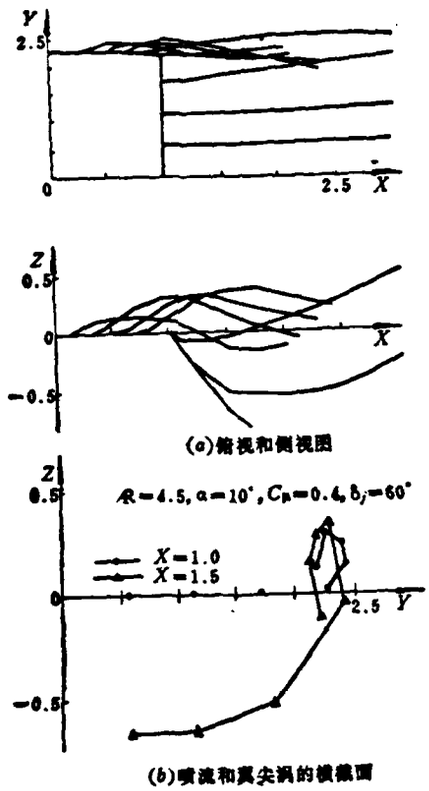

Fig. 7 The shape of jet and wing tip vertex at $\delta_j = 60°$[11]
(a) vertical and side view; (b) cross-section.

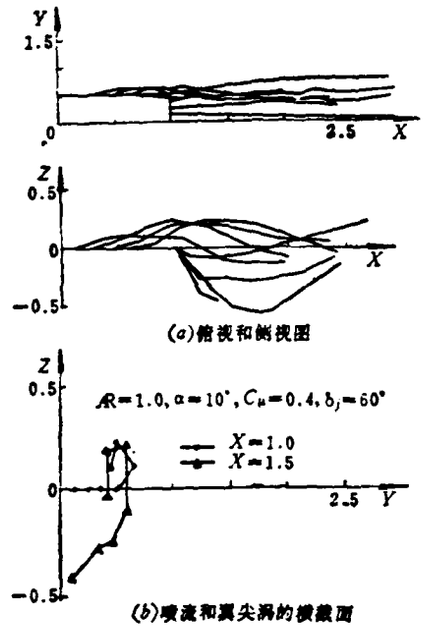

Fig. 8 The shape of jet and wing tip vertex for a small aspect-ratio wing[11]
(a) vertical and side view; (b) cross-section.

REFERENCES

[1] Spence, D. A., The Lift Coefficient of a Thin Jet Flapped Wing, Proc. Roy. Soc., Series A, 238, 1212 (1956), 46～68.

[2] Halsey, N. D., Methods for the Design and Analysis of Jet-Flapped Airfoils, AIAA paper 74—188 (1974).

[3] Sato, J., Discrete Vortex Method of Two-Dimensional Jet Flaps, AIAA J., 11, 7 (1973), 968～973.

[4] Maskell, E. C., and Spence, D. A., A Theory of the Jet Flap in Three Dimensions, Proc. Roy. Soc., Series A, 251 (1959), 407～425.

[5] Das, A., Theoretische und Experimen telle Untersuchungen an Strahlklappen-flugen, Teil I. Untersuchungen an Rechtechflugeln von Verschieden Seitenverhartnissen, Institute fur Aerodynamik der DFL, Rept. 61～11 (1961).

[6] Shen, C. C., Lopez, M. L., and Wasson, N. F., Jet-Wing Lifting-Surface Theory Using Elementary Vortex Distribution, J. Aircraft, 12.5 (1975), 448～456.

[7] Vortex Lattice Utilization, Workshop held at NASA Langley R. C., NASA SP-405, (1976).

[8] Uchiyama, N., Moulden, T. H., and Wu, J. M., "An Analysis of Various Fin Geometries and

Their Influence on Rocket Performance", Proc. of the 12th International Symp. on Space Tec. and Science (1977), 109~120.

[9] Rom, J., Almosnino, D., and Zerea, C., "Calculation of the Non-linear Aerodynamic Coefficients of Various Shapes and Their Wakes, Including Canard Configurations", Proc. of the 11 th ICAS (1978), 1, 333~344.

[10] Rom, J., Zerea, C., and Gerdon, R., "On the Calculation of Non-linear Aerodynamic Characteristic and the Near Vortex Wake", Proc. of 9th ICAS (1974), 1, 214~225.

[11] Chen, Z. L., and Wu, J. M., "Jet Wing Vortex Lattice Theory with Nonlinear Wake and Tip Flows", AIAA paper 83—0263 (1983).

NUMERICAL COMPUTATION OF TWOPHASE TURBULENT COMBUSTION PROCESSES

by

Zhou Xiaoqing
(Shengyang Aeroengine Institute)

ABSTRACT

The mathematical models and numerical methods are presented for computer prediction of aeroengine combustor flows and characteristics. Among these models the droplet turbulent diffusion model, the modified k-ϵ turbulence model and the hybrid Arrhenius/EBU model are described. The Eulerian scheme is used to construct conservation equations of both gas phase and droplet phase flows. The self-compiled computer code GEMCHIP programmed by author is provided, which incorporates SIMPLER and DROPLET algorithms for gas flow and droplet flow predictions, respectively. The block correction technique is adopted to facilitate iteration convergence. The predicted results for three typical twophase flows are given to show the applicability of this method.

Received July 3, 1984.

1. INTRODUCTION

To date, research and development on aeroengine combustors are based mainly on testing while making semi-empirical analysis subsidiary. Great advances in computation-combustion science have been made in recent years, and numerical computation has become an important technique for combustor research and designs.

This paper presents mathematical models for twophase turbulent combustion processes; gives the conservation equations of various governing processes; and describes the algorithms proposed and adopted by the author,[1-3] which are embodied in a numerical ellipse compute code, GEMCHIP for multiphase combustion, heat exchange and inter-diffusion flows. This compute code can deal with single- and two-phase stable flows in Cartesian coordinates or cylindrical coordinates; laminar or turbulent flows; cold or chemical reaction flows; and pre-mixed or diffusion flames. Results of sample computation under flow conditions for some combustors are given.

2. MATHEMATICAL MODELS OF THE PHYSICAL PROCESSES

2.1. Fog Model

Rosin-Rammler functions are often used to calculate the initial distribution of droplet size.

$$f_{n,l}=\frac{dN_l}{dr_l}=\frac{N_l S}{r_{lm}}\,\frac{\Gamma((t+4)/S)^{(t+1)/S}}{\Gamma((t+1)/S)^{(t+4)/S}}\left(\frac{r_l}{r_{lm}}\right)^t \times \exp\left\{-\left(\frac{r_l}{r_{lm}}\right)^t\left[\frac{\Gamma((t+4)/S)}{\Gamma((t+1)/S)}\right]^S\right\} \qquad (1)$$

where N_l is density of the total droplet number; S and t, the fogging parameters; r_l, the radius of droplets; r_{lm}, volumetric mean of the droplet radius; and Γ, Gama function.

In the numerical computation, $n_{i,k}$ is used to replace $f_{n,l}$

$$n_{l,k}=\int_{r_{l,\,K-\frac{1}{2}}}^{r_{l,\,K+\frac{1}{2}}} f_{n,l}\,dr_l \tag{2}$$

2.2. Droplet Turbulent Diffusion Model

Previous computations only considered the orbital motion of droplets. In fact, droplets diffuse turbulently under the influence of turbulent air mass. The following droplet turbulent diffusion model has been proposed by the author, based on Ward's analytical work. 363

$$\sigma_{n_l}=\psi\sigma_g \tag{3}$$

$$\psi=1+\sum_{m=1}^{3} b_m\left(\frac{\rho_l}{\rho_g^{3/4}}\,\frac{\epsilon}{k}r_l^2\right)^m \tag{4}$$

where σ_{nl} and σ_g are turbulent Schmidt number of droplet and that of gas, respectively; k and ϵ are the turbulence dynamic energy and dissipation rate, respectively; and ρ_l and ρ_g are the density of droplet and that of gas, respectively.

2.3. Twophase Turbulent Model

The author has considered the turbulent energy exchange between gas phase and droplet phase, and proposed a turbulent model, based on k-ϵ relation. In the model, the coupled equations for droplet phase turbulence are

$$\overline{\delta n_l \delta\vec{V}_g}=-\frac{\mu_T}{\rho_g\sigma_g}\nabla n_l \tag{5}$$

$$\overline{\delta n_l \delta\vec{V}_l}=-\frac{\mu_T}{\rho_l\sigma_{n_l}}\nabla n_l \tag{6}$$

where δn_l, $\delta\vec{V}_g$ and $\delta\vec{V}_l$ are density of droplet number, the turbulent pulse heights of the gas flow rate and the droplet velocity, respectively. The ratio of the droplet turbulent dynamic energy to that of the gas flow is $k_l/k\approx\psi^{-2}$, , thus, eqn. k can be revised

as $$\nabla\cdot(\theta\rho_g\vec{V}_g k)=\nabla\cdot\left[\theta\frac{\mu_{eff}}{\sigma_k}\nabla k\right]+\theta G_k-\theta\rho_g\epsilon-\nabla\cdot\int_0^{m_l}k_l\vec{V}_l dm_l \tag{7}$$

where $G_k=\bar{\bar{\tau}}_T:\nabla\vec{V}_g$.

Eqn. ϵ does not need revision.

2.4. Droplet Vaporization and Combustion Model

The rate of the droplet size change during vaporization and combustion is $$\frac{dr_l}{dt}=-\frac{\lambda}{\rho_l c_p}\frac{N_u\Phi_r}{r_l} \tag{8}$$

where $$N_u=1+0.276Re^{1/2}S_c^{1/3}$$

$$\Phi_r=\ln(1+B)$$

$$B=\begin{cases}\frac{1}{L}\left[\int_{T_b}^{T_g}c_p dT+\frac{q^0 Y_{ox}}{W_{ox}\nu_{ox}}\right] & \text{(油珠燃烧)-6}\\ \frac{1}{L}\int_{T_b}^{T_g}c_p dT & \text{(油珠蒸发)-7}\end{cases}$$

where 6-droplet combustion; and 7-droplet vaporization.

In the above equation, Y_{OX} is the oxygen mass concentration; W_{OX}, the molecular weight; ν_{OX}, the chemical equivalent coefficient; L and q^O are the latent heat and calorific value for vaporization of combustible oil, respectively; and Re and Sc are Reynolds number and Schmit number, respectively.

2.5. Gas Phase Turbulent Combustion Model

Let us assume that combustion is a single-step chemical reaction, i.e.,

$$\nu_F F+\nu_{ox}O\rightarrow\nu_p P \tag{9}$$

The combustion rate is the smaller one between the rates of the gas phase reaction process (calculated with Arrhenius equations) and turbulent mixing process (calculated using EBU model).

$$R_F=-\min(|R_{F,EBU}|,\ |R_{F,Ar}|) \tag{10}$$

where

$$R_{F,EBU} = -c_R \theta \rho_g k^{1/2} \left[\left(\frac{\partial Y_F}{\partial X_1} \right)^2 + \left(\frac{\partial Y_F}{\partial X_2} \right)^2 + \left(\frac{\partial Y_F}{\partial X_3} \right)^2 \right]^{1/2}$$

$$R_{F,Ar} = -B_r T_g^n \rho_g^2 Y_F Y_{ox} \exp(-E/R_u T_g)$$

where E is the activation energy; R_u is gas constant; and Y_F is the mass concentration of the combustible material.

3. COUPLED PARTIAL DIFFERENTIAL EQUATIONS OF THE GOVERNING PROCESSES

367

The controllong partial differential equations for twophase turbulent binary chemical reaction flow can be summed up as the following two forms:[3]

$$\frac{1}{\bar{r}^i}\left[\frac{\partial}{\partial \bar{x}}\left(\bar{r}^i \bar{f}_x \bar{\xi} - \bar{r}^i \Gamma_\xi \frac{\partial \bar{\xi}}{\partial \bar{x}}\right) + \frac{\partial}{\partial \bar{r}}\left(\bar{r}^i \bar{f}_r \bar{\xi} - \bar{r}^i \cdot \Gamma_\xi \frac{\partial \bar{\xi}}{\partial \bar{r}}\right)\right] = S_\xi + S_{INT} \tag{11}$$

$$\frac{1}{\bar{r}^i}\left[\frac{\partial}{\partial \bar{x}}(\bar{r}^i \bar{f}_x \bar{\xi}) + \frac{\partial}{\partial \bar{r}}(\bar{r}^i \bar{f}_r \bar{\xi})\right] - \frac{\bar{\xi}}{\bar{r}^i}\left[\frac{\partial}{\partial \bar{x}}(\bar{r}^i \bar{f}_x) + \frac{\partial}{\partial \bar{r}}(\bar{r}^i \bar{f}_r)\right] = S_{INT} \tag{12}$$

where $\bar{\xi}$ is any dimensionless flow variable; S_ξ and S_{INT} are source of action terms within one phase and between two phases; subscript, i is the coordinate factor, which is 0 in Cartesian coordinates and 1 in cylindrical coordinates.

Table 1 and 2 list all dimensionless partial differential equations in either form (11) or form (12).

4. METHOD OF NUMERICAL COMPUTATION

Equations (11) and (12) were separated into finite difference equations using controlling volumetric technique. Interlocking grid system was used to eliminate the fluctuation of the pressure field. Wall function technique was introduced at the near-wall region where there was an effect of molecular viscosity. As shown

Table 1 Governing equations in form (11)

1—方程类型	I_α	I_ν	Γ_ξ	S_ξ	S_{INT}
2—气相质量连续	$\bar{\theta}\rho_g\alpha_g$	$\theta\rho_g\alpha_g$	1	0	$-\frac{G_g}{3}\frac{\lambda}{C_p}\sum_{h=1}^{M}\bar{r}_{I,g}^3\frac{\partial}{\partial r_{I,g}}\left(\frac{\alpha_{I,g}}{r_{I,g}}N_{wI,g}\Phi_{r,g}\right)$
3—x方向气相动量守恒	$\bar{\theta}\rho_g\alpha_g$	$\bar{\theta}\rho_g\alpha_g$	u_g	$-\frac{2}{R_g\theta_0}\mu_{eff}$	$-\frac{G_g}{3}\frac{\lambda}{C_p}\sum_{h=1}^{M}\bar{r}_{I,g}^3\alpha_{I,g}\frac{\partial}{\partial r_{I,g}}\left(\frac{\alpha_{I,g}}{r_{I,g}}N_{wI,g}\Phi_{r,g}\right)-G_D\cdot\sum_{h=1}^{M}\frac{2_g}{1+B_g}\mu\alpha_{I,g}\bar{r}_{I,g}(u_g-u_{I,g})$
4—R方向气相动量守恒	$\bar{\theta}\rho_g\alpha_g$	$\bar{\theta}\rho_g\alpha_g$	v_g	$-\frac{2}{R_g\theta_0}\mu_{eff}$	$-\frac{G_g}{3}\frac{\lambda}{C_p}\sum_{h=1}^{M}\bar{r}_{I,g}^3\rho_{I,g}\frac{\partial}{\partial r_{I,g}}\left(\frac{\alpha_{I,g}}{r_{I,g}}N_{wI,g}\Phi_{r,g}\right)-G_D\sum_{h=1}^{M}\frac{2_g}{1+B_g}\mu\alpha_{I,g}\bar{r}_{I,g}(v_g-v_{I,g})$
5—气相燃料成分守恒	$\bar{\theta}\rho_g\alpha_g$	$\bar{\theta}\rho_g\alpha_g$	Y_F	$\frac{2\theta}{R_g}\frac{\mu_{eff}}{\sigma_F}$	(1) Arrhenius law $-D_1\bar{\theta}\bar{T}_g^n\rho_g^2Y_FY_{ox}\exp\left[-\frac{E}{R_gT_0}\left(\frac{1}{T_g}-1\right)\right]$ (2) EBU model $-c_R\rho\frac{k}{\varepsilon}\theta_g\bar{K}^{1/2}\left[\left(\frac{\partial Y_F}{\partial x}\right)^2+\left(\frac{\partial Y_F}{\partial r}\right)^2\right]^{1/2}$ $-\frac{G_g}{3}\frac{\lambda}{C_p}\sum_{h=1}^{M}\bar{r}_{I,g}^3\frac{\partial}{\partial r_{I,g}}\left(\frac{\alpha_{I,g}}{r_{I,g}}N_{wI,g}\Phi_{r,g}\right)$
6—混气分数守恒	$\bar{\theta}\rho_g\alpha_g$	$\bar{\theta}\rho_g\alpha_g$	ϕ	$\frac{2\theta}{R_g}\frac{\mu_{eff}}{\sigma_\phi}$	0 $-c_\phi\frac{G_g}{3}\frac{\lambda}{C_p}\sum_{h=1}^{M}\bar{r}_{I,g}^3\frac{\partial}{\partial r_{I,g}}\left(\frac{\alpha_{I,g}}{r_{I,g}}N_{wI,g}\Phi_{r,g}\right)$

1-Type of equation; 2-Gas phase mass continuity; 3-Conservation of gas phase momentum in x direction; 4-Conservation of gas phase momentum in R direction; 5-conservation of gas fuel composition; 6-conservation of the mixed gas fraction.

1—方程类型	I_α	I_ν	$\bar{\xi}$	Γ_ξ	S_ξ	S_{INT}
7—气体能量守恒	$\bar{\theta}\rho_g u_g$	$\bar{\theta}\rho_g v_g$	ξ	$\frac{2\theta}{R_e}\frac{\mu_{eff}}{\sigma_\xi}$	$2\frac{E_\alpha}{R_e}\bar{\theta}\mu_{eff}G_\alpha$ 式中 $G_\alpha=\left[2\left(\frac{\partial u_g}{\partial z}\right)^2+2\left(\frac{\partial v_g}{\partial r}\right)^2+2\left(\frac{v_g}{r}\right)^2+\delta(i)+\left(\frac{\partial u_g}{\partial r}+\frac{\partial v_g}{\partial z}\right)^2\right]$	$-G_\alpha\lambda\sum_{k=1}^{M}N_{\omega l,k}(T_g-T_{l,k})\rho_{l,k}n_{l,k}\delta(T_{l,k})-\frac{L_{ig}}{3}\left(\frac{\psi^0}{W_g}-\bar{L}\right)\frac{\lambda}{c_p}\sum_{k=1}^{M}\bar{r}^0_{l,k}\frac{\partial}{\partial r_{l,k}}\left(\frac{n_{l,k}}{r_{l,k}}N_{\omega l,k}\Phi_{r,k}\right)+G_D E_\alpha\sum_{k=1}^{M}\left\{\frac{6\mu n_{l,k}}{1+B_q}\rho_{l,k}[(u_g-u_{l,k})^2+(v_g-v_{l,k})^2]\right\}$
8—K方程	$\bar{\theta}\rho_g u_g$	$\bar{\theta}\rho_g v_g$	$\bar{K}$	$\frac{2\theta}{R_e}\frac{\mu_{eff}}{\sigma_k}$	$\frac{2}{R_e c_R}\bar{\theta}\mu_T G_\alpha-\tau_{TR}\bar{\theta}\rho_g\bar{\epsilon}$	$-L_{mR}\sum_{k=1}^{M}\bar{r}^0_{l,k}\frac{1}{\rho^g}\left[\frac{\partial}{\partial z}(\rho^g n_{l,k}a_{l,k}\bar{K}_{l,k})+\frac{\partial}{\partial r}(\rho^g\cdot n_{l,k}a_{l,k}\bar{K}_{l,k})\right]$
9—ε方程	$\bar{\theta}\rho_g u_g$	$\bar{\theta}\rho_g v_g$	$\bar{\epsilon}$	$\frac{2\theta}{R_e}\frac{\mu_{eff}}{\sigma_\epsilon}$	$\frac{c_1\tau_R}{\tau_{TR}}\bar{\theta}K\rho_g G_\alpha-c_2\tau_{TR}\bar{\theta}\rho_g\frac{\epsilon^2}{K}$	0
10—分组液滴数密度方程	$n_{l,k}$	$n_{l,k}$	$n_{l,k}$	$\frac{2}{R_l}\frac{\mu_T}{\rho_g v_g\psi}$	$\frac{G_\alpha}{3L_{mR}}\frac{\lambda}{c_p}\frac{\partial}{\partial r_{l,k}}\left(\frac{N_{\omega l,k}}{r_{l,k}}n_{l,k}\Phi_{r,k}\right)$	0

1-Type of equation; 7-Conservation of gas energy; 8-K equation; 9-ϵ equation; 10-Equation of the group droplet number density.

Table.2 Governing equations in form (12)

1— 方程类型	$\bar{\xi}$	Γ_ξ	ρ_ξ	$S_{\xi VT}$
2— x 方向油滴动量方程	$u_{l,q}$	$n_{l,q}\mu_{l,q}$	$n_{l,q}\rho_{l,q}$	$\frac{G_D}{L_{mR}(1+B_q)}$ $\frac{3_p\mu R_{l,q}}{r_{l,q}^2}(u_g-u_{l,q})$
3— R 方向油滴动量方程	$v_{l,q}$	$n_{l,q}\mu_{l,q}$	$n_{l,q}\rho_{l,q}$	$\frac{G_D}{L_{mR}(1+B_q)}$ $\frac{3_p\mu R_{l,q}}{r_{l,q}^2}(v_g-v_{l,q})$
4— 油滴温度分布	$T_{l,q}$	$n_{l,q}\theta_{l,q}$	$n_{l,q}\rho_{l,q}$	$\frac{G_v(1-T_{l0}/T_{g0})}{L_{mR}}$ $\frac{c_{pg}}{c_l}$ $\frac{\lambda N_{uc,q}R_{l,q}}{r_{l,q}^2}(T_g-T_{l,q})$

5— 式中 $c_1=1.44$, $c_2=1.92$, $c_\mu=0.09$, $c_R=1.07$; $\sigma_l=\sigma_{0_m}=\sigma_0=\sigma_k=0.7$, $\sigma_g=0.9$, $\sigma_q=1.0$, $\sigma_\varepsilon=1.3$, $L_{mR}=\frac{\rho_{l0}}{\rho_{g0}}\frac{1-\theta_0}{\theta_0}$, $\tau_{TR}=\frac{c_0R_0}{K_0u_{g0}}$, $c_R=\frac{K_0}{u_{g0}^2}$,

$R_e=\frac{2u_{g0}R_0\rho_{g0}}{\mu_0}$, $R_{em}=\frac{2u_{g0}r_{lm0}\rho_{g0}}{\mu_0}$, $E_u=\frac{P_{g0}}{\rho_{g0}u_{g0}^2}$, $E_c=\frac{u_{g0}^2}{Jc_{pg0}(T_{g0}-T_{l0})}$, $P_e=(2u_{g0}R_0c_{\rho0}\rho_{g0})/\lambda_0G_v=4\pi\frac{\lambda_0}{c_{\rho0}}\frac{N_{l,0}r_{lm,0}R_0N_{ul,0}}{\theta_0\rho_{g0}u_{g0}}$,

$G_D=6\pi\frac{\mu_0R_0r_{lm,0}N_{l,0}\alpha_0}{\theta_0\rho_{g0}u_{g0}}$, $G_v=\frac{4\pi}{1-(T_{l0}/T_{g0})}\frac{N_{ul,0}r_{lm,0}N_{l,0}R_0^2}{\theta_0P_e}$, $D_l=\frac{R_0}{u_{g0}}B_qT_{g0}^2\rho_{g0}\frac{1}{W_{0_m}}\exp(-E/(R_gT_0))$

$\delta(T_{l,q})=\begin{cases}0, & \text{若 } T_{l,q}\geqslant T_0\\ 1, & \text{若 } T_{l,q}<T_0\end{cases}$, $\delta(i)=\begin{cases}0, & \text{若 } i=0\\ 1, & \text{若 } i=1\end{cases}$, $N_{ul,0}=1+0.276R_{em}^{1/2}\left|1-\frac{u_{l,0}}{u_{g,0}}\right|^{1/2}S_{c,0}^{1/3}$; $\alpha_0=1+0.15(2r_{lm0}\rho_{g0}|u_{g0}-u_{l0i}/\mu_0)^{0.687}$

1-Type of equation; 2-Equation of droplet momentum in x direction;
3-Equation of droplet momentum in R direction; 4-Droplet temperature equation;
and 5-where.

in Fig. 1, a regular grid system with the block-off region was used to simulate the irregular contours of the combustor and the stabilizer. For the calculation of the gas phase flow field, SIMPLER algorithm was used, which saves 1/3 to 1/2 time as compared with SIMPLE algorithm, and relaxes the requirements of the subrelaxation factor.[3,5] The convection/diffusion flux on the controlling volumetrical surface was computed using power law program. The line-by-line three-vertical-angle matrix algorithm capable of direction-changing and to-and-fro scanning was used together with the block correction technique to speed up the convergence and improve the solution stability.

An algorithm called DROPLET was developed by the author for droplet flow field estimation. This algorithm uses power law for the droplet number density, and wind-facing method to calculated the flux at the intersection plane for the droplet velocity and temperature.

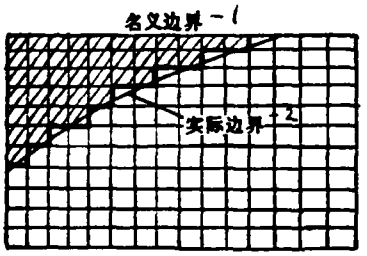

Fig. 1 Block-off region in a regular grid system

1-nomial boundary; and 2-real boundary.

GEMCHIP code has contained the above algorithm. The code is devided into two part: (1) General; and (2) For the User. The first part lists the basic algorithms and the second one has

corresponding changes based on the type of problems, geometrical shape, boundary and entrance conditions, and grid arrangement. The operation sequence of GEMCHIP is as follows: firstly, the gas phase flow field (without droplets) was computed using SIMPLER, which was taken as the primary guessing of the gas-phase field for two-phase flow calculation. Secondly, the droplet field was computed using DROPLET. Also obtained were the exchange quantities of mass, energy and momentum between gas and liquid phases. These construct the source term, S_{INT} in the gas-phase equation and can be substituted back to SIMPLER to correct gas phase field. Then, DROPLET was re-entered. This kind of alternation was performed until the convergent criterion for both gas and oil phase flow fields was satisfied.

5. APPLICATIONS

GEMCHIP code has been applied to various cases, such as single-phase and binary-phase aerodynamics, heat transfer, combustion and chemical reactions. In this section, only three samples will be given due to limited space.

5.1. Two-phase Cold Flow[6]

Fig. 2 shows the flow parameter distributions for the gas-phase and droplet phase in the axial direction. It is shown that the smaller the droplet size, the smaller the velocity difference between droplets and gas flow. Fig. 3 shows the medium-size droplet volumetric fraction curves for the two-phase flow of a stream of combustible oil gushing from the center of a truncated cone.

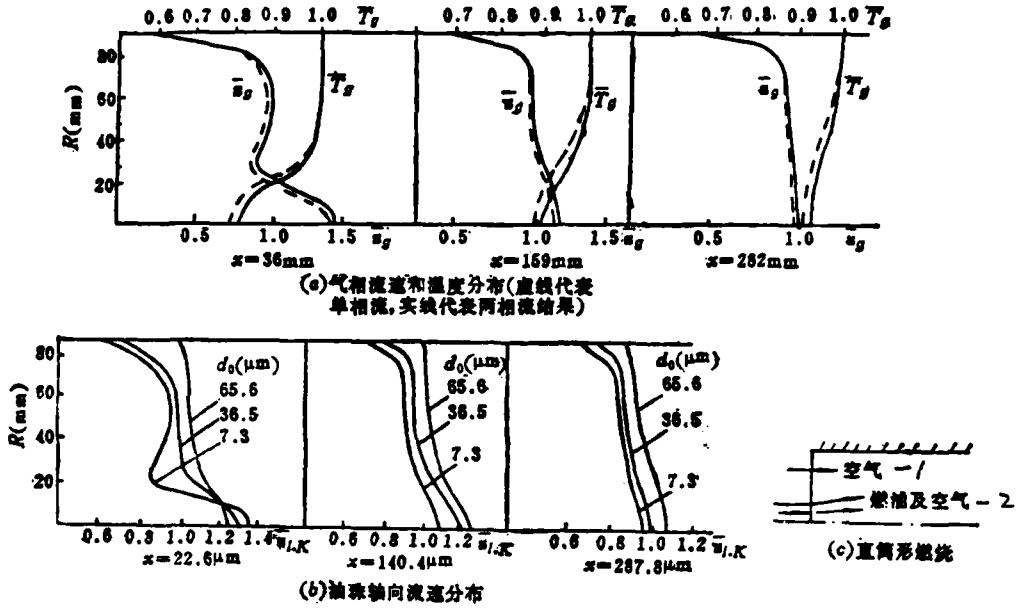

(a)气相流速和温度分布(虚线代表单相流,实线代表两相流结果)

(b)油珠轴向流速分布

(c)直筒形燃烧

图 2　直筒形燃烧室中的两相冷流流场

Fig. 2　Twophase cold flow fields in a cylindrical combustor

(a) Gas-phase flow rate and temperature distribution (dash lines represent single-phase flow and solid lines, two-phase flow).

(b) Droplet flow rate distribution in the axial direction.

(c) Cylindrical combustor. 1-air; 2-combustible oil and air.

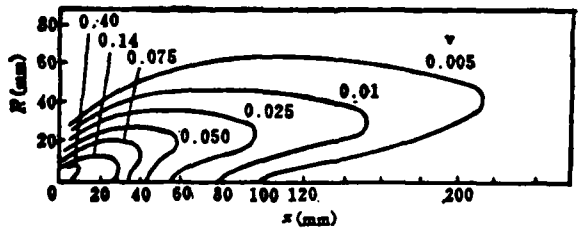

图 3　油珠容积含量的等值线

Fig. 3　Isograms of droplet volumetric fraction

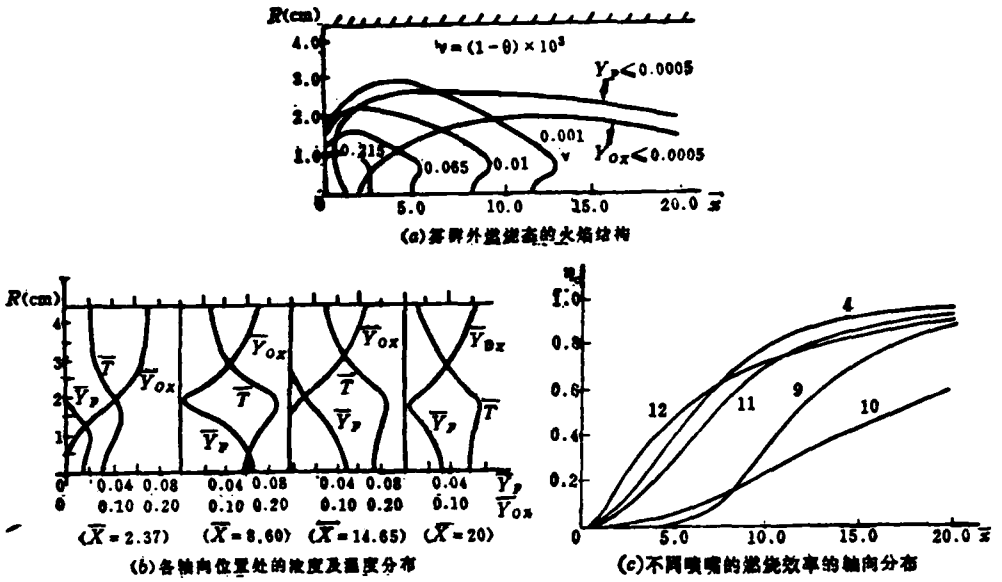

图 4　直筒形燃烧室中的两相燃烧流场

Fig. 4　Twophase combustion flow fields in a cylindrical combustor

(a) Structure of the flame in combustion state outside the dust fog.

(b) Concentration and temperature distributions in the axial direction.

(c) The axial distribution of the combustion efficiency for various nozzles.

5.2. Two-phase Combustion in a Cylindrical Combustor[7]

Fig. 4(a) shows the flame structure. The flame is mainly located outside the oil dust fog. Fig. 4(b) gives the axial distributions of the combustible material, oxygen concentration and temperature at the cross-section. Fig. 4(c) gives the axial distribution of combustion efficiency under various working conditions.

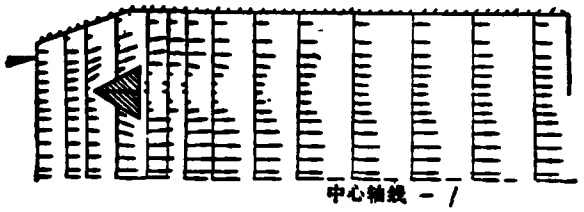

图 5　两相燃烧加力室中的气相速度矢量图

Fig. 5　Gas phase hodograph in a twophase combustion afterburner

1-axis.

5.3. Two-phase Combustion in the Afterburner

Fig. 5 gives the gas-phase hodograph for the afterburner of a small culvert-ratio fan engine with a parallel inlet gas mixer/pressurizer and a stabilizer with single-row v-shaped slots. The figure clearly shows the structure of the return air region and the flow acceleration due to combustion. It is shown that the influence of the return air region extended to the lower reach.

6. CONCLUSIONS

369

The method and GEMCHIP code presented in this paper have been successfully applied to several typical flows in combustors. Two-phase ternary code is expected to be developed from this work to compute performances of real main combustors and complicated afterburners. A close combination of numerical computation with engineering testing and semi-empirical analysis will greatly improve research and development on combustors.

REFERENCES

[1] Launder, B. E. and Spalding, D. B. "The Numerical Computation of Turbulent Flow" Comp. Methods Appl. Mech. Eng., Vol.3, (1974).

[2] Spalding, D. B. "Mathematical Models of Turbulent Flames, A Review" Combustion Science and Technology Vol. 13, (1975).

[3] Zhou, X. Q. and Chiu, H. H. "The Numerical Methods in Twophase Turbulent Flows and the New Computer Code GEMCHIP" Internal Report of University of Illinois at Chicago, (1983).

[4] Ward, P., Collings, N. and Hay, N., "A Comparison of Simple Models of Turbulent Droplet Diffusion Suitable for Use in Computa-tions of Spray Flames" ASME 82-WA/HT-2.

[5] Patankar, S. V., "Numerical Heat Transfer and Fluid Flows" Mc Graw-Hill, (1980).

[6] Zhou, X. Q. and Chiu, H. H., "Turbulent Spray Group Evaporation and Combustion" 9th International Colloquium on Dynamics of Explosion and Reactive System, Poiter, France, (1983).

[7] Zhou, X. Q. and Chiu, H. H., "Spray Group Combustion Processes in Air Breathing Propulsion Combustors" AIAA-83-1323, AIAA/ASME/SAE 19th Joint Propulsion Conference, (1983).

GUST ALLEVIATION USING COMBINED CONTROL LAWS

by

Chang Jin
(Northwestern Polytechnical University)

ABSTRACT

An analytical method of gust alleviation and other active control purposes (relaxed static stability etc.) for an airplane is described. Gust alleviation uses direct measurements of atmospheric turbulence to yield a feed-forward or open-loop control law. It is relatively insensitive to changes in flight conditions. Thus a combined control law can be obtained which contains feed-back and feed-forward components.

The stability of the gust alleviation system and the performances of other active control purpose can be satisfied by obtaining a linear optimal control defined by a quadratic performance index. Thus the performance index is combined. and the optimal feed-back control law is straightforward and well-known.

An application of the combined control law to a flexible airplane is presented. Calculations have been performed to obtain the normal acceleration responses of the airplane to the turbulence and the state responses for the other active control purpose.

Received March 1, 1984.

INTRODUCTION

One of the subjects which need to be studied for some airplanes is gust alleviation. Considering that the application of active control technology (ACT) to airplanes is usually malfunctional, to combine them economically and effectively is a subject worth considering. In this paper, it is suggested to alleviate airplane response to gust by using an open-loop system with direct gust measurement. The requirements for other active control functions can be met with a feed-back system. The combined control laws for combined gust alleviation and other active control purposes are discussed.

One of the difficult problems which one faces in the airplane gust alleviation system designs is the sensitivity, i.e., big changes in the system parameters with flight speed and altitude. The advantage of an open-loop system with direct gust measurement is its low sensitivity. Though the open-loop system has its shortcomings, an improved performance can be obtained by combining an open-loop with a closed-loop in the system.

1. PARTIAL STATE ALLEVIATION FOR DIRECT GUST MEASUREMENT

The airplane motion equation under the assumption of linearization and small perturbation is

$$\dot{x}(t)=Fx(t)+Gu(t)+Jw_g(t) \tag{1}$$

where x(t) is the state vector; u(t), input vector; $w_g(t)$, gust disturbance; and F, G, and J are nxn, nxm, and nxp constant matrices. In order to eliminate the effect of gust on airplane when $w_g(t)$ was

measured,[1] the following equation should be satisfied:

$$Gu(t)+Jw_g(t)=0 \tag{2}$$

However, matrix G is usually a square matrix and its inverse can not be obtained. Thus, the control law, u(t) can not be solved directly. We transformed matrix F in eqn. (1) to a diagonal matrix and assumed the transformed matrix as T, then $\tilde{x}=Tx$. Thus, eqn. (1) could be written as

$$\dot{\tilde{x}}=TFT^{-1}\tilde{x}+TGu+TJw_g=\overline{\Lambda\tilde{x}}+TGu+TJw_g \tag{3}$$

where Λ is a diagonal matrix with complex numbers in it. For convenience, transformation $\hat{x}=M\tilde{x}$ was performed to eliminate complex numbers in Λ, where

$$M=\left[\begin{array}{cccc:c}
1 & 1 & & & \\
-\frac{1}{j} & \frac{1}{j} & & 0 & \\
 & & \ddots & & 0 \\
 & & & 1 & 1 \\
 & 0 & & -\frac{1}{j} & \frac{1}{j} \\
\hdashline
 & & 0 & & I
\end{array}\right]\begin{array}{l}\left.\begin{array}{l}\\\\\\\\\end{array}\right\}\text{复特征根部分}-3\\ \left.\begin{array}{l}\\\end{array}\right\}\text{实特征根部分}-4\end{array} \tag{4}$$

In (4), 3-complex characteristic root; and 4-real characteristic root.

Then, eqn. (1) was changed to

$$\dot{\hat{x}}=MTFT^{-1}M^{-1}\hat{x}+MTGu+MTJw_g \tag{5}$$

$$MTFT^{-1}M^{-1}=\bar{\Lambda}=\left[\begin{array}{cccc:c}
\sigma_1 & \omega_1 & & & \\
-\omega_1 & \sigma_1 & & 0 & \\
 & & \ddots & & 0 \\
 & 0 & & \sigma_r & \omega_r \\
 & & & -\omega_r & \sigma_r \\
\hdashline
 & & 0 & & \begin{array}{cc}\lambda_{r+1} & \\ & \ddots \\ 0 & \lambda_n\end{array}
\end{array}\right] \tag{6}$$

(1). Ref. 4 discusses the methods for the gust measurement and the measures to reduce the measurement errors. Results of flight tests under various flight conditions are given.

where σ_i and ω_i are the real part and the imaginary part of the ith complex characteristic root. Eq. (6) has r complex characteristic root and n-r real ones. Choose m state variables $\hat{x}_1(t)$ in $\hat{x}(t)$, which play a major role in gust alleviation. The rest n-m state variables are $\hat{x}_2(t)$.[1] Eqn. (5) can be written as

$$\begin{Bmatrix} \dot{\hat{x}}_1 \\ \dot{\hat{x}}_2 \end{Bmatrix} = \begin{bmatrix} \bar{\Lambda}_1 & 0 \\ 0 & \bar{\Lambda}_2 \end{bmatrix} \begin{Bmatrix} \hat{x}_1 \\ \hat{x}_2 \end{Bmatrix} + \begin{bmatrix} G_1 \\ G_2 \end{bmatrix} \{u\} + \begin{bmatrix} J_1 \\ J_2 \end{bmatrix} \{w_g\} \tag{7}$$

where $\begin{bmatrix} \bar{\Lambda}_1 & 0 \\ 0 & \bar{\Lambda}_2 \end{bmatrix}$ is similar to $\bar{\Lambda}$, the only difference between them being the different arrangement. $\begin{bmatrix} G_1 \\ G_2 \end{bmatrix}$, and $\begin{bmatrix} J_1 \\ J_2 \end{bmatrix}$ are similar to MTG and MTJ, respectively, but the arrangement is different. If the following equation can be satisfied

$$[G_1]\{u\} + [J_1]\{w_g\} = 0 \tag{8}$$

where G_1 is an mxm square matrix and it is not singular, the control law is

$$\{u\} = -[G_1]^{-1}[J_1]\{w_g\} \tag{9}$$

The airplane motion equation can be divided into

$$\begin{aligned} \{\dot{\hat{x}}_1\} &= [\bar{\Lambda}_1]\{\hat{x}_1\} \\ \{\dot{\hat{x}}_2\} &= [\bar{\Lambda}_2]\{\hat{x}_2\} + ([J_2] - [G_2][G_1]^{-1}[J_1])\{w_g\} \end{aligned} \tag{10}$$

$\{\hat{x}_1\}$ is independant of gust and $\{\hat{x}_2\}$ is influenced by the gust disturbance. This makes the $\{\hat{x}_1\}$-related part of the gust response alleviated.

2. ALLEVIATION OF THE OUTPUT VECTORS

It is of significance to alleviate airplane's measurable outputs (such as acceleration). The airplane motion and output equations are

$$\left.\begin{aligned} \dot{x}(t) &= Fx(t)+G_1u_1(t)+Jw_g(t) \\ y_1(t) &= C_1x(t)+D_1u_1(t)+Ew_g(t) \end{aligned}\right\} \tag{11}$$

To alleviate output vector $y_1(t)$, the following equation should be satisfied: 381

$$y_1(t)=C_1x(t)+D_1u_1(t)+Ew_g(t)=0 \tag{12}$$

Generally, D_1 is not a square matrix and has no inverse. However, the generalized inverse can be found based on the matrix geometrical normal number and eqn. (12) can be approximately satisfied, that is, making the following equation

$$\|C_1x+D_1u_1+Ew_g\|^2_{Q_1}=(C_1x+D_1u_1+Ew_g)^TQ_1(C_1x+D_1u_1+Ew_g)=y_1^TQ_1y_1 \tag{13}$$

reach a minimum value. In this case, Q_1 is a symmetrical and normal weighing matrix which shows the alleviation weighing effect for various elements in $y_1(t)$. Find the partial derivative of eqn. (13) with respect to u_1 and make it equal to zero; we get

$$2D_1^TQ_1D_1u_1+2D_1^TQ_1C_1x+2D_1^TQ_1Ew_g=0 \tag{14}$$

Solve u_1, and the control law is

$$u_1=-(D_1^TQ_1D_1)^{-1}D_1^TQ_1(C_1x+Ew_g) \tag{15}$$

If $y_1^TQ_1y_1$ in eqn. (13) is replaced by $y_1^TQ_1y_1+u_1^TR_1u_1$, the process of finding the generalized inverse has already considered the requirements for the controlled energy. R_1 is a symmetrical and normal weighing matrix which controls the energy weighing quantity at the control surface. The corresponding control law[2] is

$$u_1=-(D_1^TQ_1D_1+R_1)^{-1}D_1^TQ_1(C_1x+Ew_g) \tag{16}$$

Under the gust measurement conditions, eqns.(15) and (16) contain feed-forward component $(D_1^TQ_1D_1+R_1)^{-1}D_1^TQ_1Ew_g$ and feed-back component $(D_1^TQ_1D_1+R_1)^{-1}\times D_1^TQ_1C_1x$. The latter component can possibly make the system unstable. A stabilization term can be added

to the feed-back component using the extreme point arrangement or optimum regulator to ensure the stability of the overall system, as shown in the following sample calculation.

When combining gust alleviation with other active control purposes, assume the airplane motion and output equations as

$$\dot{x}=Fx+G_2u_2 \qquad y_2=C_2x+D_2u_2 \tag{17}$$

where u_2 is the control output satisfying other major active control purposes, which may involve an operating surface different from that of gust alleviation. Other active control performance indices can be written as second order forms, such as

$$V=\min_{u_2}\frac{1}{2}\int_0^\infty (y_2^TQ_2y_2+u_2^TR_2u_2)dt \tag{18}$$

where Q_2 and R_2 are symmetrical and normal weighing matrices. Combining the performance index, equation (18) with the feed-back component which ensures the stability of the gust measurement system, the combined performance index is written as

$$V'=\min_{u}\frac{1}{2}\int_0^\infty (y^TQy+u^TRu)dt \tag{19}$$

where

$$u=\begin{Bmatrix}u_1\\u_2\end{Bmatrix},\quad y=\begin{Bmatrix}y_1\\y_2\end{Bmatrix},\quad Q=\begin{bmatrix}Q_1 & 0\\0 & nQ_2\end{bmatrix},\quad R=\begin{bmatrix}R_1 & 0\\0 & mR_2\end{bmatrix} \tag{19'}$$

while n and m are the weighing factors measuring various weighing matrices of gust alleviation and other active control purposes. The combined performance index, eqn. (19) satisfies eqn. (18) and at the same time, the feed-back control makes gust alleviation stable under the conditions where $(y_1^TQ_1y_1+u_1^TR_1u_1)$ is minimum. This is because vector y in eqn. (19) contains output vector y_1.

Since linear optimal regulator control is independent of the

system's initial condition and uncontrollable disturbance, the output equation in eqn. (11) is

$$y_1 = C_1 x + D_1 u_1 \tag{20}$$

The optimal control to assume functional V' an extreme value is

$$u = -\hat{R}^{-1} G^T P x \tag{21}$$

382

where matrix P satisfies the following algebraical equation

$$\hat{F}^T P + P\hat{F} - PG\hat{R}^{-1}G^T P + \hat{Q} = 0 \tag{22}$$

where $G = \begin{bmatrix} G_1 \\ G_2 \end{bmatrix}$, . Since there is cross term when eqn. (19) is expressed in state variables, transformation is needed to cancel this term.[3] Thus, $\hat{R}$, $\hat{F}$ and $\hat{Q}$ in eqn. (22) are given as

$$\hat{R} = \begin{bmatrix} D_1 & 0 \\ 0 & D_2 \end{bmatrix}^T \begin{bmatrix} Q_1 & 0 \\ 0 & nQ_2 \end{bmatrix} \begin{bmatrix} D_1 & 0 \\ 0 & D_2 \end{bmatrix} + \begin{bmatrix} R_1 & 0 \\ 0 & mR_2 \end{bmatrix} \tag{23}$$

$$\hat{F} = F - [G_1 \; G_2]\hat{R}^{-1} \begin{bmatrix} D_1 & 0 \\ 0 & D_2 \end{bmatrix} \begin{bmatrix} Q_1 & 0 \\ 0 & nQ_2 \end{bmatrix} \begin{bmatrix} C_1 \\ C_2 \end{bmatrix} \tag{24}$$

$$\hat{Q} = \begin{bmatrix} C_1 \\ C_2 \end{bmatrix}^T \begin{bmatrix} Q_1 & 0 \\ 0 & nQ_2 \end{bmatrix} \begin{bmatrix} C_1 \\ C_2 \end{bmatrix} - \begin{bmatrix} C_1 \\ C_2 \end{bmatrix}^T \begin{bmatrix} Q_1 & 0 \\ 0 & nQ_2 \end{bmatrix} \begin{bmatrix} D_1 & 0 \\ 0 & D_2 \end{bmatrix} \hat{R}^{-1} \begin{bmatrix} D_1 & 0 \\ 0 & D_2 \end{bmatrix}^T \times \begin{bmatrix} Q_1 & 0 \\ 0 & nQ_2 \end{bmatrix} \begin{bmatrix} C_1 \\ C_2 \end{bmatrix} \tag{25}$$

Combining eqns. (16)-(21) to get combined control law

$$u = \begin{Bmatrix} u_1 \\ u_2 \end{Bmatrix} = -\hat{R}^{-1} \left(\begin{bmatrix} D_1^T Q_1 C_1 \\ 0 \end{bmatrix} + [G_1 \; G_2]^T P \right) x - \hat{R}^{-1} \begin{bmatrix} D_1^T Q_1 E \\ 0 \end{bmatrix} w_g \tag{26}$$

where the first term consists of two parts: feed-back component which alleviates output y_1 in the gust disturbance, i.e., the feed-back component in eqn. (16); and the control quantity which makes V' assume a minimum value. Because V' contains y_1 and y_2, it satisfies performance index, V and ensures stability of gust alleviation. The second term is the open-loop gust alleviation term resulted from gust measurement.

3. SAMPLE CALCULATION

Let us take the variables in the airplane rigid-body longitudinal motion equation and body's elasticity equation as its state variables. Assume that the control surface is the movable horizontal tail surface and the wing flap. If only the vertical component of the gust is considered, the airplane motion equation is

$$F=\begin{bmatrix} -1.54 & 1.0 & 0 & 0 \\ -6.0 & -1.36 & 0 & 0 \\ 0 & 0 & 0 & 1.0 \\ 0.5994 & 0 & -400.0 & 0 \end{bmatrix},\quad G=\begin{bmatrix} -0.47 & 0.328 \\ -32.2 & -8.9 \\ 0 & 0 \\ -0.3055 & -0.066 \end{bmatrix}$$

$$J=\begin{bmatrix} -0.00513 \\ -0.02 \\ 0 \\ 0.002 \end{bmatrix},\quad C_1=[-44.2544 \quad 0.648 \quad -30.58 \quad 0]$$

$$D_1=[-0.9417 \quad 14.278],\qquad E_2=[-0.1475]$$
$$C_2=[1.0 \quad 0 \quad 0 \quad 0],\qquad D_2=[0],$$

Assume the weighing matrix Q=I, and $R_1=R_2=R=10I$, we have 383

$$\hat{R}=\begin{bmatrix} 10.886 & -13.437 \\ -13.437 & 213.89 \end{bmatrix},\quad \hat{F}=\begin{bmatrix} -0.499 & 0.985 & 0.719 & 0 \\ -25.596 & -1.073 & -13.541 & 0 \\ 0 & 0 & 0 & 1.0 \\ 0.4667 & 0.00194 & -400.917 & 0 \end{bmatrix}$$

$$\hat{Q}=\begin{bmatrix} 119.658 & -1.738 & 82.1 & 0 \\ -1.738 & 0.03 & -1.212 & 0 \\ 82.1 & -1.212 & 56.776 & 0 \\ 0 & 0 & 0 & 0.001 \end{bmatrix}$$

The combined control law is

$$u=\begin{Bmatrix} \delta_e \\ \delta_f \end{Bmatrix}=-\begin{bmatrix} -2.515 & -0.33 & 0.723 & -0.0199 \\ -3.074 & 0.019 & -1.957 & -0.00095 \end{bmatrix}x-\begin{bmatrix} 0.00064 \\ -0.00981 \end{bmatrix}w_g$$

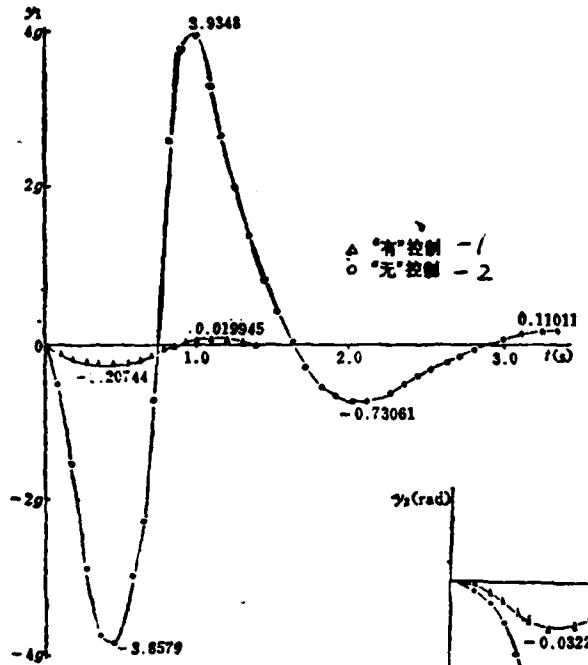

图1 对输出 y_1(垂直加速度) 的响应

Fig. 1 The response of output y_1 (normal acceleration)

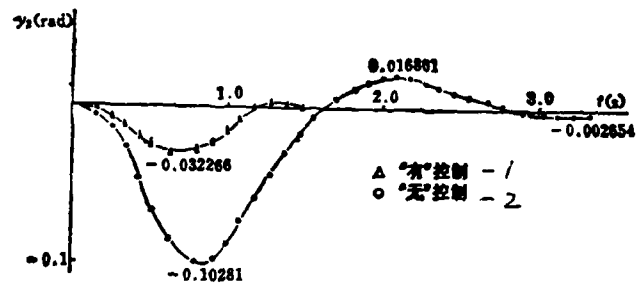

图2 对输出 y_2(其他主动控制性能) 的响应

Fig. 2 The response of output y_2 (other active control purpose)

1-with control

2-no control

Assume gust as $u(1-\cos\omega t)$, and calculate the plane's response to gust. Results are shown in Figs. 1 and 2, which compare two different conditions: under control and without control. In calculation, it was assumed u=20 m/sec and ω=6.2852.

4. CONCLUSIONS

A gust measurement technique for gust alleviation are suggested for airplanes with various active control purposes. The combined control laws given in this paper can meet the requirements for gust alleviation and other active control purposes. Response calculation was performed for an airplane, based on combined control laws. Calculation results and data comparison show obvious advantages of these combined laws.

REFERENCES

[1] Rynaski, E.G., Andrisani, D. and Eulrich, J., Gust Alleviation Using Direct Turbulence Measurements, AIAA 79-1674.

[2] Rynaski, E.G., Gust Alleviation-Criteria and Control Laws, AIAA 79-1676.

[3] Chang Jin, Random Analysis of Gust Alleviation Systems, Scientific Data, Northweatern Polytechnical University, SHj 8201.

[4] Krag.B., Active Control Technology for Gust Alleviation. Von Karman Institute for Fluid Dynamics Lecture Series 1979-1.

CALCULATION OF SUPERSONIC FLOWS AROUND A THREE-DIMENSIONAL WING AND A WAISTED BODY WITH CHARACTERISTIC METHOD IN STREAM SURFACE COORDINATES

by

Wang Baoyu

(Beijing Institute of Aeronautics and Astronautics)

ABSTRACT

According to the exact characteristic surface equation of three dimensions and the physical relations along bicharacteristics in stream surface coordinates of Ref. 1, the pressure distributions of circula-elliptic delta wing and waisted body are calculated with "real" characteristic method. The results are compared with those of Refs. 2, 3, 4 and 6.

Received June 25, 1984.

1. INTRODUCTION

In 1960's, Bulter[4] first performed numerical calculations for inviscid supersonic flow around a circular-elliptic wing at Ma_∞=3.5. He simplified the equations by using high supersonic characteristic, and obtained surface pressure distribuions. His results agree well with the experimental data. In 1974, Walkden and Caine[2,3] calculated the same wing using stream surface coordinates, and found discrepancy between Bulter's results and theirs. The characteristic equation and relations of physical property variations along characteristics (three-dimensional) on which Ref. 2 and 3 were based are all approximate. Since the term of the partial derivative of the dependent variable with respect to ξ^3 was moved to the right side of the equation in Ref. 5, the characteristic equation obtained was not three-dimensional, but equivalent to two-dimensional. Moreover, Ref. 2 and 3 used two relations of the physical property variations along characteristics to replace two relations in the coupled aerodynamic equations, and solved these equations using difference method, not the characteristic method. Such an equation solving method is still open to question. In Ref. 2, the calculation results with different steps were interpolated to obtain a zero mesh. Ref. 3 mentioned that calculation could not be continued near the front fringe, but Ref. 2 did not mention this.

The author obtained an accurate three-dimensional characteristic equation in stream surface coordinates and an accurate relation of the physical property variations along four characteristics over two sets of stream surfaces, $\xi^3=C^3$ and $\xi^2=C^2$.[1] In the

present study, this "real" characteristic method was used to solve the flow fields of circular-elliptic delta wing and waisted body. The author also obtained a general characteristic relation for three-dimensional separated flow in the arbitrary curve and stream surface coordinates.[8] Considering the relation given in Ref. 1 is lengthy, it is not given here.

2. CALCULATION METHOD

The calculation method used in this study is the characteristic method choosing $\xi^1=x^1$ in a stream surface coordinate system. If the aerodynamic properties at the surface where $\xi^1=x^1=C^1$ have been caculated, various dependent variables at point A, which is on surfaces $\xi^3=C^3$, $\xi^2=C^2$ and $\xi^1+\Delta\xi^1$, need to be calculated. The calculation procedures for space points and boundary points are as follows:

(1) Space points. Let us take four points on the intersections of $\xi^3=C^3$, $\xi^2=C^2$ and $\xi^1=C^1$ (Fig. 1) (i.e., points 6, 7, 8 and 9 at

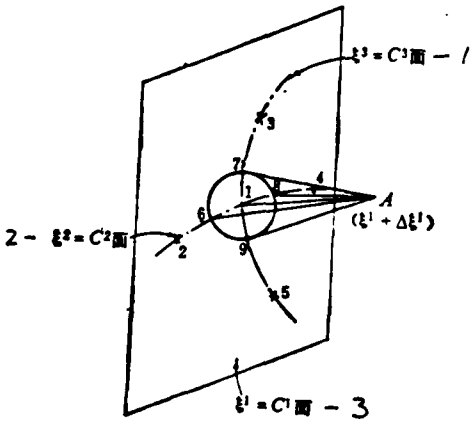

图1 流面与双特征线

Fig. 1 Stream surface and bicharacteristics

1-surface $\xi^3=C^3$;

2-surface $\xi^2=C^2$;

3-surface $\xi^1=C^1$.

which the aerodynamic parameters can be solved by interpolating values at point 1 and points 2, 3, 4 and 5) to construct a mesh cone (characteristic cone) passing through A (using one-by-one approximation technique). Then, take points 6, 7 and 9 as one group and points 7, 8 and 9 as another to solve the aerodynamic parameters at A, $(p)_{A1}, (t_1^2)_{A1}, (t_1^3)_{A1}$ and $(p)_{A2}, (t_1^2)_{A2}, (t_1^3)_{A2}$. Parameters at point A are the averages of the corresponding values from each group. Thus, if the aerodynamic parameters at calculation points 1, 2, 3, 4 and 5 on surface $\xi^1=\overline{x^1=C^1}$ are known, various parameters at point A on surfaces $\xi^1=C^1$, $\xi^2=C^2$ $\xi^1+\Delta\xi^1$, can be solved.

(2) Boundary points. The calculation method for the boundary points are similar to that for the space points. The relation between t_1^2 and t_1^3 at A is known. For point 5 and 9 on surface $\xi^1=C^1$ (Fig. 1), use point 6 and 7, and point 7 and 8 to determine p and t_1^2 at point A and then to arrange the corresponding two values.

Calculation was also conducted for a waisted body (axial symmetry, two-dimensional). Similar calculation method was used. There were no space points 6 and 8. The unknowns to be determined were only p and t_1^2; There was only boundary point 7, and p was the only parameter to be determined.

In this method, C.F.L. conditions must be satisfied in order to make $\Delta\xi^1$ small enough, otherwise unstability would appear during calculation. Such an unstability did occur in our axial symmetrical flow calculations. There was no unstability found in the delta wing calculation, since $\Delta\xi^1$ selected has been small enough.

3. CALCULATION RESULTS AND DISCUSSION

(1) Circular-elliptic delta wing ($\alpha=0^{\circ}$). The geometrical shape of this "subsonic" front fringe wing can be found in Ref. 3. After assuming the steps as $\Delta\xi^1=\Delta x^1=0.003985$, $\Delta\xi^2=0.0063754$, $\Delta\xi^3=0.19635$, the surface pressure distributions on the tangential surfaces $x^1=0.417$ and 0.683 were calculated. Results are shown in Figs. 2 and 3.

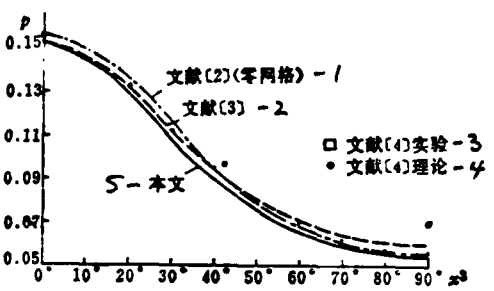

图2 在$x^1=0.417$处机翼的表面压强

Fig. 2 Surface pressure of wing at $x^1=0.417$

1-Ref. 2 (zero mesh); 2-Ref. 3; 3-Ref. 4, test; 4-Ref. 4, theory; 5-this work.

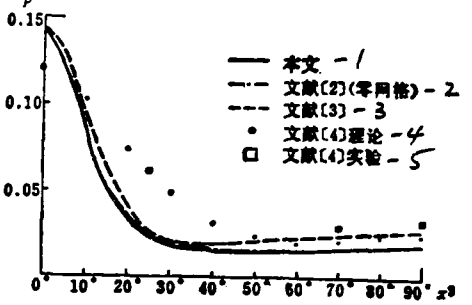

图3 在$x^1=0.683$处的机翼表面压强

Fig. 3 Surface pressure of wing at $x^1=0.683$

1-this work; 2-Ref. 2 (zero mesh); 3-Ref. 3; 4-Ref. 4, theory; 5-Ref. 4, test.

Generally, these results agree fairly well with those given in Ref. 2 and are slightly lower than those in Ref. 3. The characteristic equation and the relations of the physical property variations along the bicharacteristics on which the present work was based are correct and the calculation method is a "real" characteristic one; while the relations on which Ref. 2 and 3 were based are approximate, and the methods used are not "real" characteristic ones (but approximate relations of the physical property variations along the characteristics were used). The difference due to this is conceivable. The "zero mesh" in Ref. 2 contains "real" characteristic method which eliminates the difference from the

395

approximation algorithm. Thus, a good agreement between the results of this work and those given in Ref. 2 is obtained. The calculation with different steps in Ref. 2 shows that the smaller the step, the lower the pressure (see Fig. 3 and 5 therein). From this, it can be understood why the author's results are slightly smaller than those presented in Ref. 3.

(2) The axial symmetrical flow around a waisted body ($\alpha=0^{\circ}$). Compared with Ref. 6, this work gives smaller values of pressure distribution. They are also smaller than those given in Ref. 7 (Fig. 4). Near $x^1=0.4$ and in $x^1=0.7$-1.0 region, difference in pressure distribution is appreciable (but still very small). The starting equations in this work and Ref. 6 are correct. In Ref. 6, the algorithm is not a "real" characteristic one and there was no "zero mesh" obtained.

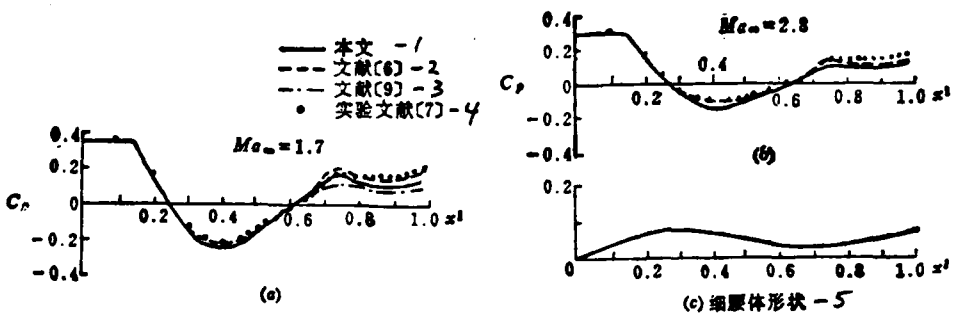

图4 细腰体的表面压强及其形状

Fig. 4 Surface pressure and shape of waisted body

1-this work; 2-Ref. 6; 3-Ref. 9; 4-test, Ref.7; 5-shape of waisted body.

The author thanks Zhang Qinan, who did a lot of work at the beginning of the computation, and Qian Yiji, who provided the compute code for the Taylor-Maccoll solution to flow around a cone.

REFERENCES

[1] Wang Baoyu and Zhang Qinan, Coupled Aerodynamic Equations for Inviscid Steady Flows with Constant Specific Heat in Stream Surface Coordinates and Their Characteristic Equations, Scientific Research Reports, Beijing Institute of Aeronautics and Astronautics, BH-B360(1978).

[2] Walkden, F. and Caine, P., Surface Pressure on a Wing Moving with Supersonic Speed. Proceedings of the Royal Society of London, Vol. 341, Nov. (1974), pp. 177~193.

[3] Walkden, F. and Caine, P., A Shock Capturing Method for Calculating Supersonic Flow Fields, A. R. C. C. P. 1290, (1974).

[4] Bulter, D. S., The Numerical Solution of Hyperbolic Systems of Partial Differential Equations in Three Independent Variables, Proceedings of The Royal Society A, Vol. 255, April(1960), pp. 232~252.

[5] Walkden, F., A Form of the Supersonic Flow Equation for an Ideal Gases., A. R. C. R&M 3757, (1974).

[6] Walkden, F. and Caine, P., Application of a Pseudoviscous Method to the Calculation of the Steady Supersonic Flow Past a Waisted Body, International Journal for Numerical Method in Engineering, Vol. 5, (1972), pp. 151~162.

[7] Winter, K. G., Rotta, J. C. and Smith, K. G., Studies of the Turbulent Boundary Layer on a Waisted Body of Revolution in Subsonic and Supersonic Flow, A. R. C. R&M 3633.

8 Wang Baoyu, General Characteristic Relations of Three-dimensional Supersonic Flow in Arbitrary Curve and Stream Coordinates, Acta Aerodynamica Sinica, No. 2, pp. 1-16(1982).

[9] Jackson, C. M. and Smith, R. S., A Method for Determing the Total Drag of Pointed Body of Revolution in Supersonic Flow with Turbulent Boundary Layer, NASA TN D-5046, (1969).

THERMODYNAMIC ANALYSIS OF TURBOFAN ENGINES

by

Cui Jiya

(Beijing Institute of Aeronautics and Astronautics)

ABSTRACT

Based on the thermodynamic principles, a mixed exhaust turbofan cycle is split into an inner "regenerative" subcycle and an outer simple subcycle (Fig. 2) with the borrowed work (Eq. 2) and the borrowed heat (Eq. 3) refunded to the inner subcycle. The performance of the engine is shown to be composed of subcycles' performances through respective fraction ratios α and β as in Eqs. 4~10. Fig. 3 gives a thorough view of the energy and efficiency relation in the subcycles as well as for the whole engine. The illustrated example in Table 1 indicates that, although combined with an efficient inner regenerative subcycle, a low compression and low heating outer subcycle gives a thermal efficiency inferior to the corresponding simple jet engine. The overall efficiency, thrust and specific fuel consumption are better only due to high propulsive efficiency. The respective functions of two subcycles in the engine are thus elucidated.

Received January 5, 1984.

1. INTRODUCTION

Since 1960's, turbofan engines have been extensively developed due to their low fuel consumption. However, only a little analysis of their principles[1-5] has been conducted so far, most of which are in terms of the overall engine performance. In the present paper, the engines are split up into inner and outer subcycles, based on the principles of self-induced compression work and heating, and examples are given to show the practical thermodynamic performances of each subcycle. The simplified solutions of the pressure ratios for three compressors with optimum major performances are obtained, based on the fixed specific heat of the overall engine. The results can be used as a reference for analysis and designs.

2. SEPARATED EXHAUST TURBOFAN ENGINES

Though a dual-functional process can be expressed in a temperature-entropy diagram (Fig. 1), there is no heat source in

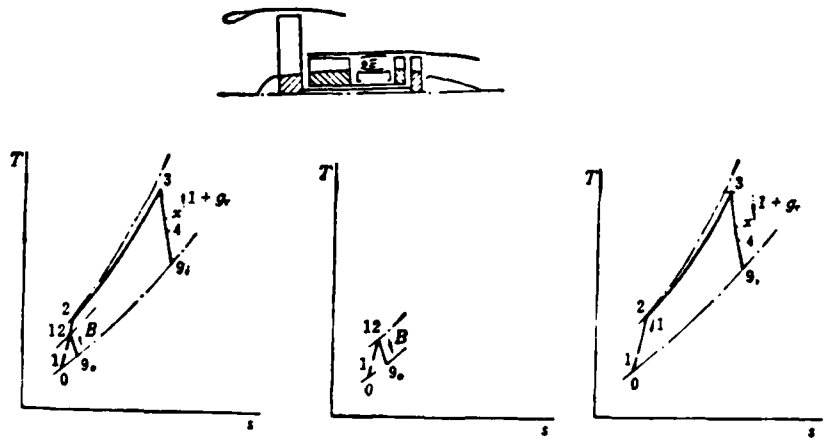

图1 分排涡扇发动机（状态点除0、9外均指总参数，下同）

Fig. 1 Separate Exhaust Turbofan (State points except 0, 9 refer to total parameters, same in Fig. 2)

the outer, and a cycle does not occur, based on the second law of thermodynamics. Thus, analysis can not be done on it. However, the propulsive efficiency can be divided into the ratios of propulsive work to effective work for the inner stream and outer stream.

$$\eta_p = \frac{P}{W} = \frac{\frac{1}{1+B}W_i}{W}\ \frac{P_i}{W_i} + \frac{\frac{B}{1+B}W_0}{W}\ \frac{P_0}{W_0} = \alpha_w \eta_{pi} + \beta_w \eta_{p0} \qquad (1)$$

where α_w and β_w are the effective work part ratio of the inner stream of flow, and that of the outer stream of flow, respectively.

It is shown from the sample calculation in Table 1 that since there exists flow resistance due to the turbo and fan when the effective work is transferred toward the outer function, the thermal efficiency of turbofan engines is lower than that of the corresponding turbo engines. The reason for an improvement of their efficiency, propulsion and fuel consumption is the improved propulsive efficiency due to separated stream of the low-speed jet.

3. MIXED TURBOFAN ENGINES

An approximate analysis was conducted based on the constant-overall-pressure mixing. The same analysis can also be used for varying-overall-pressure mixing. Fig. 2 shows the thermodynamic process which was split up into inner and outer subcycles. The outer compression "borrowed work" from the inner

$$W_{bor.} = B\Delta i_{1\sim 11} J/\eta_m = (1+g_r)\Delta i_{12} J \qquad (2)$$

and the outer also "borrowed heat" from the inner (i.e., borrowed fuel Bg_{r1})

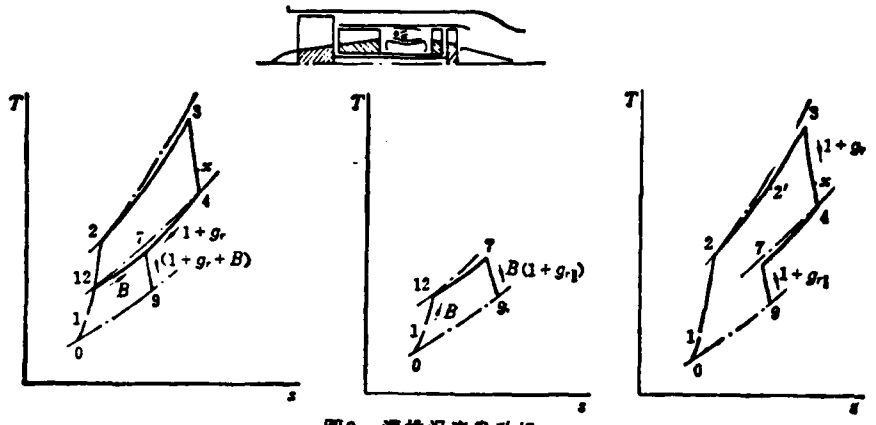

图2 混排涡扇发动机

Fig. 2 Mixed Exhaust Turbofan

$$Q_{bor.}=Bg_{r1}H_r\xi J=B\Delta i_{12-7}J=(1+g_r)\Delta i_{47}J=\Delta i_{12}'J \qquad (3)$$

The inner was equivalent to the regenerative subcycle before the tail jet. Interestingly enough, such a regeneration made the temperature at the exit of cold flow higher than that at the entrance of the hot flow ($T_2'>T_4$).

Fig. 3 gives the energy relations. For settling accounts of the inner and outer subcycle performance, it is only required to set out the "borrowed work" and "borrowed heat" respectively.

$$W=\underbrace{\frac{1}{1+B}}_{\alpha_G}\underbrace{\left[\underbrace{\frac{(1+g_{r1})c_9^2-V^2}{2g}}_{W_1'}+W_{bor.}\right]}_{W_1}+\underbrace{\frac{B}{1+B}}_{\beta_G}\underbrace{\left[\underbrace{\frac{(1+g_{r1})c_9^2-V^2}{2g}}_{W_9}-W_{bor.}/B\right]}_{W_1} \qquad (4)$$

$$\eta_t=\frac{W}{g_rH_rJ/1+B}=\underbrace{\frac{g_{r1}}{g_r}}_{\alpha_Q}\underbrace{\frac{W_1'}{g_{r1}H_rJ}}_{\eta_{t1}}+\underbrace{\frac{Bg_{r1}}{g_r}}_{\beta_Q}\underbrace{\frac{W_1}{g_{r1}H_rJ}}_{\eta_{t1}} \qquad (5)$$

$$P=\underbrace{\frac{1}{1+B}}_{\alpha_G}\underbrace{\left[\underbrace{\frac{(1+g_{r1})c_9-V}{g}\cdot V+W_{bor.}}_{P_1'}\right]}_{P_1}+\underbrace{\frac{B}{1+B}}_{\beta_G}\underbrace{\left[\underbrace{\frac{(1+g_{r1})c_9-V}{g}\cdot V-W_{bor.}/B}_{P_1}\right]}_{P_1} \qquad (6)$$

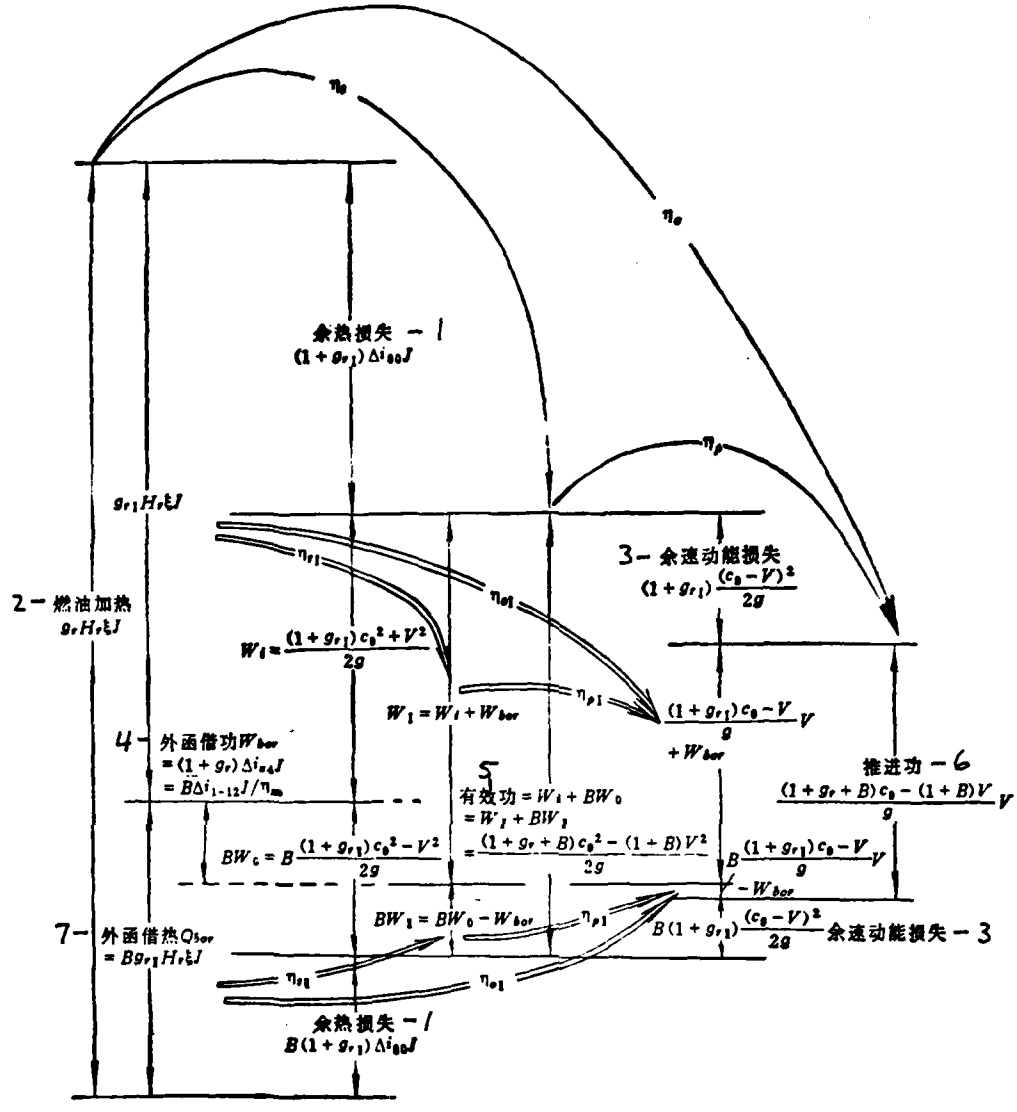

图3 分循环能量关系

Fig. 3 Energy Flow Chart of Subcycles

1-space heat loss; 2-combustible oil heating; 3-remaining speed kinetic energy loss; 4-outer function's borrowed work; 5-effective work; 6-propulsive work; 7-outer function's borrowed heat.

Note: The effective work minus the remaining speed kinetic energy loss is still smaller than the propulsive work, the difference being $g_{r1}\frac{V^2}{2g}$及$Bg_{r1}\frac{V^2}{2g}$. The energy was replenished by the kinetic energy of the fuel during flight.

Table 1 Examples of Performance Composition

($H \geqslant 11$km, $M=0.9$, $T_3^*=1358$K, $\eta_{jk}=0.99$, $\eta_j^*=0.841$, $H_r=10300$, $\xi=0.97$, $\sigma_r=0.96$, $\pi_k^*=19.05$, $\eta_k^*=0.778$, $\eta_T^*=0.925$, $\eta_m=0.99$, $\eta_{pk}=0.9725$, $\sigma_{mix}=0.97$)

	η_s	η_p
1—涡喷发动机	46.39%	44.80%
2—分排涡扇 $B=5$ $\frac{c_{qo}}{c_{qi}}=0.77$	39.81%	3—内涵 $0.3105\times67.73\%$ $0.6895\times78.92\%$ } 75.45% 4—外涵
5—混排涡扇 $B=0.7$ $\pi_j^*=3.328$	6—内分循环 $0.6854\times55.28\%$ $0.3146\times29.75\%$ } 47.25% 7—外分循环	$0.8019\times65.54\%$ $0.1981\times2.66\%$ } 53.08%

η_0	R_{sw}	$\frac{R}{G_I}$	C_R
20.78%	69.40	69.40	1.0455
30.04%	16.72	100.32	0.723
$0.6854\times36.23\%$ $0.3146\times0.79\%$ } 25.08%	$\frac{1}{1.7}\times82.92$ $\frac{0.7}{1.7}\times1.187$ } 49.27	83.75	0.9901×0.5998 0.0099×27.46 } 0.8664

1-turbo engine; 2-separated exhaust turbofan; 3-inner stream; 4-outer stream; 5-mixed exhaust turbofan; 6-inner subcycle; and 7-outer subcycle.

$$\eta_p = \frac{P}{W} = \underbrace{\frac{\frac{1}{1+B}W_1}{W}}_{\alpha_W} \underbrace{\frac{P_1}{W_1}}_{\eta_{p1}} + \underbrace{\frac{\frac{B}{1+B}W_1}{W}}_{\beta_W} \cdot \underbrace{\frac{P_1}{W_1}}_{\eta_{p1}} \qquad (7)$$

$$\eta_o = \frac{P}{\frac{g_r H_r J}{1+B}} = \eta_t \eta_p = \underbrace{\frac{g_{r1}}{g_r}}_{\alpha_Q} \underbrace{\frac{P_1}{g_{r1} H_r J}}_{\eta_{o1} = \eta_{t1}\eta_{p1}} + \underbrace{\frac{\beta g_{r1}}{g_r}}_{\beta_Q} \underbrace{\frac{P_1}{g_{r1} H_r J}}_{\eta_{o1} = \eta_{t1}\eta_{p1}} \qquad (8)$$

where α and β are the corresponding part ratios. Accordingly, the unit propulsion and unit fuel consumption are

$$R_{dw} = \underbrace{\frac{1}{1+B}}_{\alpha_G} \underbrace{\left[\frac{(1+g_{r1})c_9 - V}{g} + \frac{W_{bor.}}{V}\right]}_{R_{dw1}} + \underbrace{\frac{B}{1+B}}_{\beta_G} \underbrace{\left[\frac{(1+g_{r1})c_9 - V}{g} - \frac{W_{bor./B}}{V}\right]}_{R_{dw1}} \qquad (9)$$

$$C_K = \underbrace{\frac{\frac{1}{1+B}R_{dw1}}{R_{dw}}}_{\alpha_K} \underbrace{\frac{g_{r1} \times 3600}{R_{dw1}}}_{C_{R1}} + \underbrace{\frac{\frac{B}{1+B}R_{dw1}}{R_{dw}}}_{\beta_R} \underbrace{\frac{g_{r1} \times 3600}{R_{dw1}}}_{C_{R1}} \qquad (10)$$

respectively.

It can be seen from the sample calculation in Table 1 that in terms of thermal efficiency, regeneration improved the inner subcycle; however, low pressure and low temperature made the outer subcycle worse, so that the engine performed only slightly better than the corresponding turbo jet engine. It is the high propulsive efficiency which made the overall efficiency, propulsion (expressed by R/G_1) and fuel consumption superior to those of a turbo jet engine. Since the heat and kinetic energy of the gas flow in the outer function was not fully used, the unit propulsion of the turbofan engine, R_{dw} is lower than that of a turbo jet.

After slight adjustment, the subcycle method can be used to outer-functional afterburning, mixing afterburning and dual-functional afterburning engines. However, when designing and analyzing the optimum parameters for a turbofan engine, a simple way is to take the overall engine's performance into account.[1-3]

4. SIMPLIFIED ANALYTICAL METHOD

In this study, the specific heat was assumed for engine's overall process. Then, the performance parameters were solved.

The condition for dual functional constant-overall-pressure mixing is

$$T_3^*\left[1-\left(\frac{\pi_f^*}{\pi_k^*\sigma_r}\right)^{\frac{k-1}{k}}\right]\eta_T^*=T_1^*\left[\frac{\pi_k^{*\frac{k-1}{k}}-1}{\eta_k^*}+B\frac{\pi_f^{*\frac{k-1}{k}}-1}{\eta_f^*}\right]$$

Assume $x=\pi_k^{*\frac{k-1}{k}}$, $f=\pi_f^{*\frac{k-1}{k}}$ and $B'=B\eta_k^*/\eta_f^*$, $C=T_1^*/T_3^*\eta_T^*\eta_k^*$, $\tau_r=\sigma_r^{\frac{k-1}{k}}$,

then we have the fan pressure ratio

$$f=\frac{(1+C+B'C)x-Cx^2}{B'Cx+1/\tau_r} \tag{11}$$

When $\frac{df}{dx}=0$, $B'C^2x^2+(2C/\tau_r)x-(1+C+B'C)/\tau_r=0$.

From that, x_f was solved for the compressor pressure ratio $(\pi_k^*)_{x_f^*}$ with the maximum fan pressure ratio (which means an optimum afterburning propulsion and lowest fuel consumption):

$$x_f=\frac{-1+\sqrt{1+B'(1+C+B'C)\tau_r}}{B'C\tau_r} \tag{12}$$

If the overall pressure loss in the combustor and the difference between the compressor efficiency and fan efficiency were not taken into account ($\sigma_r=1=\tau_r$ and $B'=B$), then, the equation could be simplified into A.M. Lyul'ka's equation[4].

After dual functional mixing

$$T_7^*=\frac{T_2^*+BT_{12}^*}{1+B}=\frac{T_2^*+BT_1^*}{1+B}=\frac{T_3^*-T_1^*(\pi_k^{*\frac{k-1}{k}}-1)/\eta_k^*+BT_1^*}{1+B}$$

$$=\underbrace{\frac{T_3^*+(B+1/\eta_k^*)T_1^*}{1+B}}_{P}-\underbrace{\frac{T_1^*}{\eta_k^*(1+B)}}_{Q}x$$

Assume $\tau=\pi_r^{\frac{k-1}{k}}$, $\pi_{mix}=\sigma_{mix}^{\frac{k-1}{k}}$, then the temperature decrease of the tail jet was $\Delta T_{7*}^*=\eta_{mt}(P-Qx)\left(1-\frac{1}{\tau\tau_{mix}f}\right)$

$$= \eta_{pt}(P-Qx)\frac{x^2-\overbrace{\{1+B'(1-1/\tau\tau_{mix})+1/C\}}^{G_1}x+\overbrace{1/\tau\tau_{mix}\tau_r C}^{G_2}}{\underbrace{x^2-(1+B'+1/C)x}_{G_3}}$$

The unit propulsion was

$$R_{dw}=\left\{\sqrt{2gc_pJ\eta_{pt}\left[\frac{(P-Qx)(x^2-G_1x+G_2)}{x^2-G_3x}\right]}-V\right\}/g \tag{13}$$

From $\frac{d\{\ \}}{dx}=0$ in eqn. (13), x_R of the compressor pressure ratio $(\pi_k^*)_R$ when the propulsion was maximum was

$$\overbrace{x^4-2G_3x^3-\left(\frac{G_1-G_3}{Q}P+G_2-G_1G_3\right)x^2+2G_2\frac{P}{Q}x-G_2G_3\frac{P}{Q}}=0 \tag{14}$$

After test calculation, x had only one real root from 1 to 3.727 $(\pi_k^*=100)$.

The fuel consumption rate was

$$C_R=\frac{T_3^*-T_1^*(1+(\pi_k^{*\frac{k-1}{k}}-1)/\eta_k^*)}{1+B}\ \frac{c_p}{\xi H_r}\ \frac{3600}{R_{dw}}$$

$$=\frac{\overbrace{T_3^*-T_1^*(1-1/\eta_k^*)}^{K}-\overbrace{(T_1^*/\eta_k^*)x}^{S}}{R_{dw}}\ \frac{3600c_p}{(1+B)\xi H_r} \tag{15}$$

$$=\frac{3600}{(1+B)\xi H_r}\sqrt{\frac{c_pg}{2J}}\left\{\frac{K-Sx}{\sqrt{\eta_{pt}\frac{(P-Qx)(x^2-G_1x+G_2)}{x^2-G_3x}}-\underbrace{V/\sqrt{2gc_pJ}}_{V_1}}\right\}$$

From $\frac{d\{\ \}}{dx}=0$ in eqn. (15), when the fuel consumption rate was minimum, $(\pi_k^*)_{C_R}$, x_C was

$$\sqrt{\frac{(P-Qx)(x^2-G_1x+G_2)}{x^2-G_3x}}\left(\sqrt{\frac{(P-Qx)(x^2-G_1x+G_2)}{x^2-G_3x}}-\frac{V_1}{\sqrt{\eta_{pt}}}\right)$$

$$+\frac{Q\left(x-\frac{K}{S}\right)\left[x^4-2G_3x^3-\left(\frac{G_1-G_3}{Q}P+G_2-G_1G_3\right)x^2+2G_2\frac{P}{Q}x-G_2G_3\frac{P}{Q}\right]}{2(x^2-G_3x)^2} \tag{16}$$

$$=0$$

After test calculation with equation of higher degree, x only had one real root from 1 to 3.727. 403

The sample performance calculations are given in Fig. 4 and Table 2. In the case of accurate solutions with varying specific

Table 2 Variation of Performance with Compressor Pressure Ratio.

1—定比热 (c_p = 0.24 k = 1.4) 简化解 η_k^* = 0.778 2′ η_T^* = 0.925				3—变比热准确解 $(\eta_p)_k$ = 0.848 $(\eta_p)_T$ = 0.91			
π_k^*	π_j^*	$\frac{R}{G_1}$	C_R	π_k^*	π_j^*	$\frac{R}{G_1}$	C_R
2.97	1.791	67.7	1.2632	3.62	1.991	77.4	1.1769
4.93	2.244	74.1	1.0727	4.93	2.271	81.1	1.0768
6.90	2.530	76.1	0.9857	6.23	2.477	82.9	1.0164
8.87	2.720	76.6	0.9328	8.85	2.753	83.9	0.9442
12.26	2.911	75.8	0.8754	12.25	2.947	83.1	0.8908
15.65	2.997	74.3	0.8383	15.64	3.034	81.3	0.8573
19.04	3.020	72.3	0.8119	19.04	3.057	79.2	0.8341
27.02	2.938	67.2	0.7716	25.08	3.007	75.0	0.8072
34.99	2.766	62.0	0.7484	31.12	2.894	70.7	0.7913
42.97	2.559	56.7	0.7358	37.16	2.750	66.3	0.7827
50.94	2.343	51.4	0.7317	43.20	2.592	62.0	0.7799
52.45	2.302	50.4	0.7318	48.20	2.458	58.4	0.7815
58.62	2.138	46.4	0.7357	53.20	2.323	54.9	0.7867
65.28	1.967	41.9	0.7465	58.20	2.191	51.4	0.7956
72.47	1.791	37.1	0.7679	63.20	2.061	47.8	0.8090

1-fixed specific heat; 2-simplified solution; 3-accurate solution with varying specific heat.

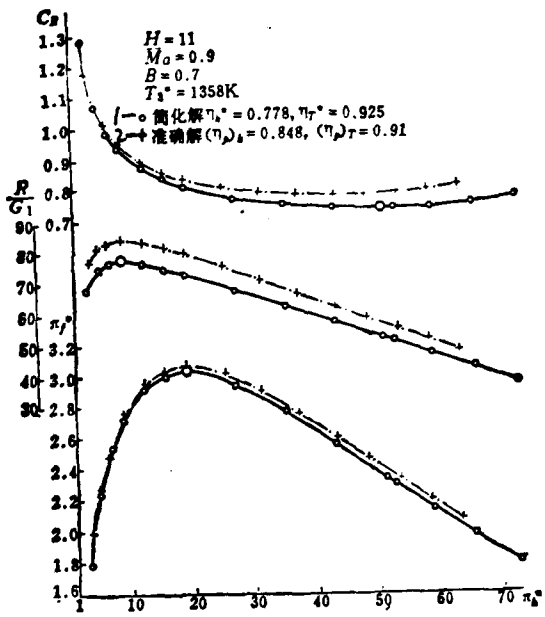

图 4 性能随压气机压比变化

Fig. 4 Variation of Performance with Compressor Pressure Ratio

1-simplified solution; and 2-accurate solution.

heat listed herein for comparison, the mechanical efficiency η_m=0.99, fuel consumption g_r, outer functional overall pressure coefficient σ_1=0.99 and tail jet efficiency η_{pk}=0.9725 were considered and the cooling air coefficients were introduced: in combustion, γ=0.91; in the turbo with compressor, γ_k=0.9456 and with fan, γ_f=0.97; In order to take into account the variations of compressor and turbo efficiencies with pressure ratios, the multivariant efficiencies equivalent to that in Table 1, $(\eta_p)_k$=0.848 and $(\eta_p)_T$=0.91 were assumed. This means that the ordered efficiency was nearly unchangable. The big circle and cross in Fig. 4 and the underlined data in Table 2 are the optimum parameters. Generally, the initial data are similar to those in Table 1.

It is shown that the simplified analysis can not only show the tendency of variations but also quickly estimate the pressure ratios of the two compressors with optimum propulsion and fan pressure ratios.

REFERENCES

1 Cui Jiya, Approximate Analytical Solutions of the Optimum Cycle Parameters for Mixed Exhaust Turbofan Engines, Journal of Engineering Thermophysics, Vol. 2, No. 2(1981).

2 Cui Jiya, Investigation on the Optimum Cycle Parameters for Mixed Exhaust Turbofan Engines, Scientific Research Report, Beijing Institute of Aeronautics and Astronautics, BH-B557(1980).

3 Cui Jiya, Liu Yan and Hu Shongyan, Improved Approximate Analytical Solutions of the Optimum Cycle Parameters for Mixed Exhaust Turbofan Engines, Journal of Engineering Thermophysics,

Vol. 4, No. 3(1983).

4. Shlyakhtenko, S.M., Sosunova, V.A. Teory of two-channel turbo-jet engines. MASHGIZ, Moscow, 1979.

5 Hartmann, A., NASA TTF 12562, Mixing Study on the Culvert Fan Jet Engines, Translated by Zhou Xiaoqing, Shengyang Aeroengine Institute(1974).

END

DTIC

6-86